1 **Distinct neurophysiological features and memory representations along the long**

2 **axis of the developing medial temporal lobe**

3 Qin Yin[1], Adam J. O. Dede[2], Robert T. Knight[3], Eishi Asano[4,5], Elizabeth L. Johnson[6],

4 Noa Ofen[1,7]

5 1. Center for Vital Longevity and Department of Psychology, School of Behavioral and

6   Brain Sciences, The University of Texas at Dallas, Dallas, TX

7 2. Departments of Medical Social Science and Neurology, Northwestern University,

8   Chicago, IL

9 3. Departments of Psychology and Neuroscience and the Helen Wills Neuroscience

10   Institute, University of California, Berkeley, CA

11 4. Department of Pediatrics and Neurology, Wayne State University, Detroit, MI

12 5. Children's Hospital of Michigan, Detroit, MI

13 6. Departments of Medical Social Science, Pediatrics, and Psychology, Northwestern

14   University, Chicago, IL

15 7. Institute of Gerontology, Wayne State University, Detroit, MI

16 Correspondence: qin.yin@utdallas.edu, noa.ofen@utdallas.edu

17

18 **ABSTRACT**

19   The medial temporal lobe (MTL) is crucial for episodic memory, whereby posterior

20 MTL preferentially represents visuospatial information, and anterior MTL is involved in

21 the representation of semantic or conceptual information. The neurophysiological

22 underpinnings of content-preferential organization in the developing MTL are largely

23 unknown. Here we utilized rare electrocorticography (ECoG) recordings from 23

24 pediatric epilepsy patients who completed a visual scene recognition memory task to

25 systematically examine the neurophysiological underpinnings of memory formation

26 along the MTL long axis. The timing of high-frequency activity (HFA, ~70-150 Hz)

27 differed between the posterior and anterior MTL, peaking after scene onset in the

28 posterior MTL and around scene category response (indoor/outdoor scene

29 categorization) in the anterior MTL. Further, in the posterior MTL, HFA was predictive of

30 successful memory formation and positively linked to memory performance, highlighting

31 the importance of posterior MTL HFA to memory formation. In contrast, theta frequency

32 in the anterior MTL was linked to memory performance, and theta-HFA phase-amplitude

33 coupling before scene category responses was predictive of successful memory

34 formation, highlighting the importance of anterior MTL theta oscillations to memory

35 formation. Our findings establish distinct neurophysiological features along the

36 posterior-to-anterior axis of the developing MTL that differentially support the

37 representation of perceptual and conceptual information during memory formation.

38 **Keywords:** electrocorticography (ECoG), medial temporal lobe (MTL), episodic

39 memory, high-frequency activity (HFA), theta oscillations, memory development

40

41 **INTRODUCTION**

42   Episodic memory, the ability to remember past experiences, is fundamental to our

43   daily life and continues to develop from childhood into adulthood[1–4]. The medial

44   temporal lobe (MTL) is essential for episodic memory formation[5,6], supporting memory

45   through a content-based manner, with visuospatial information represented in the

46   posterior region and semantic or conceptual information in the anterior region along its

47   long axis[7–9]. This content-specific organization is well-documented in adults but remains

48   largely unknown whether the developing MTL exhibits similar spatial organization and

49   how the development of this organization might contribute to memory development.

50   Human functional connectivity[10–12] and animal tract-tracing[13–15] studies reveal that

51   the posterior MTL is predominantly connected to regions of the dorsal visual pathway,

52   while the anterior MTL is predominantly connected to regions of the ventral visual

53   pathway. These differential connections may constrain how the MTL preferentially

54   represents visuospatial information, such as scenes, in the posterior region, and

55   stimulus entity, such as objects and faces, in the anterior region[7,8]. Neuropsychological

56   studies provide near-consistent observations of preferential content processing along

57   the MTL long axis, with lesions in the posterior MTL leading to impairments in scene

58   recognition and lesions in the anterior MTL resulting in deficits in recognition for items

59   such as objects and faces[9,16–21]. Neuroimaging studies, however, have yielded mixed

60   findings. While the posterior MTL consistently shows increased responses to

61   successfully remembered scenes[9,22,23], the anterior MTL exhibits memory-related

62   responses to both items (i.e., objects, faces) and scenes[24–26]. Responses to scenes in

63   the anterior MTL align with its posited role in integrating distinct visuospatial features

3

64 into higher-level representations such as conceptual categories of scenes[8,15,27–29].

65 Information feedforward from the posterior MTL to the anterior MTL may underlie the

66 association of visuospatial information in the anterior MTL for the representations of the

67 conceptual aspect of the visuospatial stimuli[13,30].

68 Systematic examination of activity along the MTL long axis may enhance our

69 understanding of MTL development. For example, some studies have reported age-

70 invariant MTL involvement for memory for visual scenes[31] or words[32], while others have

71 observed age-related increases in posterior MTL involvement for visual scenes[33,34] or

72 age-related decreases in posterior MTL involvement for objects[35]. The mixed age-

73 related differences and the well-studied content-specific organization along the MTL

74 long axis in adults raise key questions regarding whether the developing MTL exhibits

75 distinct content representations along its long axis. These questions are tightly linked to

76 investigating the underlying neurophysiology along the MTL long axis in the developing

77 brain.

78 We utilized rare subdural electrocorticography (ECoG) recordings from pediatric

79 epilepsy patients during the performance of an established scene subsequent memory

80 task[31,33,36–42] to examine the representations of indoor and outdoor visual scenes along

81 the long axis of the developing MTL during memory formation. We hypothesized that the

82 posterior MTL supports visuospatial representation of visual scenes, while the anterior

83 MTL supports conceptual category representation (i.e., whether a stimulus depicts an

84 "indoor" or "outdoor" scene). We used ECoG to define the temporal dynamics and

85 neurophysiological mechanisms associated with external scene onset and internally

86 generated scene category responses. We examined two distinct neurophysiological

4

87   features: high-frequency activity (HFA, ~70 – 150 Hz) and oscillations in the theta band

88   (~2-8 Hz). HFA indexes local neuronal activity[43–47] and positively correlates with the

89   fMRI BOLD signal[43,45,48–50], providing a measure of localized neuronal activity with high

90   temporal resolution. Theta is the predominant oscillation in the MTL and has been linked

91   to episodic memory and other MTL-dependent cognitive functions including working

92   memory and spatial navigation[51–54]. It is posited to support MTL computations involved

93   in information integration via the coordination of local activity[55–58]. In addition to

94   supporting local computation, theta also coordinates inter-regional communication and

95   information transfer[59–62]. We examined content representations in the posterior and

96   anterior MTL supporting memory formation by quantifying HFA and theta oscillations

97   associated with scene onset and scene category response onset.

98   We demonstrate that the posterior and anterior MTL are differentially involved in

99   external scene processing and internal scene category responses, as indicated by the

100   different timing of HFA in each region. The neurophysiological features associated with

101   memory differed between these two regions. The posterior MTL exhibited an HFA-

102   dependent mechanism; increased HFA predicted successful memory formation and was

103   positively linked to memory performance. In contrast, the anterior MTL exhibited a theta-

104   dependent mechanism, where theta frequency correlated with memory performance.

105   Furthermore, in the anterior MTL, increased theta-HFA phase-amplitude coupling before

106   scene category response predicted successful memory formation. Lastly, increased

107   posterior-anterior theta coupling predicted successful memory formation. Our findings

108   establish distinct content representations along the long axis of the developing MTL,

109   supported by different neurophysiological features, which, together, may underlie

110   multifaceted representations of episodic memory.

111

RESULTS

Typical memory performance in pediatric epilepsy subjects

114   We analyzed ECoG data from 23 subjects (12 females and 11 males; 5.9-20.5

115   years of age; 13.4 ± 4.0 [M ± SD] years; Table S1) who had seizure- and artifact-free

116   electrodes sampling MTL while they were performing a scene subsequent memory task

117   that has been widely used for studying the neural correlates of memory and memory

118   development[31,33,36–42]. Subjects studied sets of 40 pictures of scenes and responded

119   whether each scene was "indoor" or "outdoor" in preparation for a memory test (Fig. 1a).

120   They were then tested with the previously presented pictures intermixed with 20 new

121   pictures and responded whether they saw the pictures before or not by responding "old"

122   or "new" to each scene. During the study block, a mean of 0.94 ± 0.04 of scenes was

123   correctly identified as indoor/outdoor, indicating that subjects were proficient at correctly

124   categorizing the scenes. During the test block, 0.67 ± 0.17 of the studied scenes were

125   later recognized as "old" (i.e., hit rate), and 0.30 ± 0.17 of the new scenes were later

126   recognized as "old" (i.e., false alarm rate). Memory performance was assessed with

127   recognition accuracy, calculated as the hit rate minus the false alarm rate. Recognition

128   accuracy varied across subjects from 0.02 to 0.76, with a mean ± SD of 0.37 ± 0.21

129   (Table S1).

130   Recognition accuracy did not correlate with age in this subsample of patients with

131   MTL coverage (r = 0.20, p = 0.36; Fig. 1b). However, recognition accuracy

6

132 demonstrated a pattern of age-related increase, reaching significance in data from the

133 larger sample of epilepsy patients we collected regardless of electrode coverage (n =

134 107; r = 0.26, p = 9.8×10^{-3}; Fig. 1b). Importantly, we observed large variability in

135 recognition accuracy among adolescents aged ~12-18 years old, which is comparable

136 to the typical developmental trajectory in large non-clinical samples[31,38,39] in a similar

137 scene subsequent memory task (n = 186; r = 0.58, p = 3.91×10^{-18}; Fig. 1b). Altogether,

138 the behavioral pattern suggests typical memory development in our clinical sample,

139 allowing us to investigate neurophysiological signatures supporting memory formation in
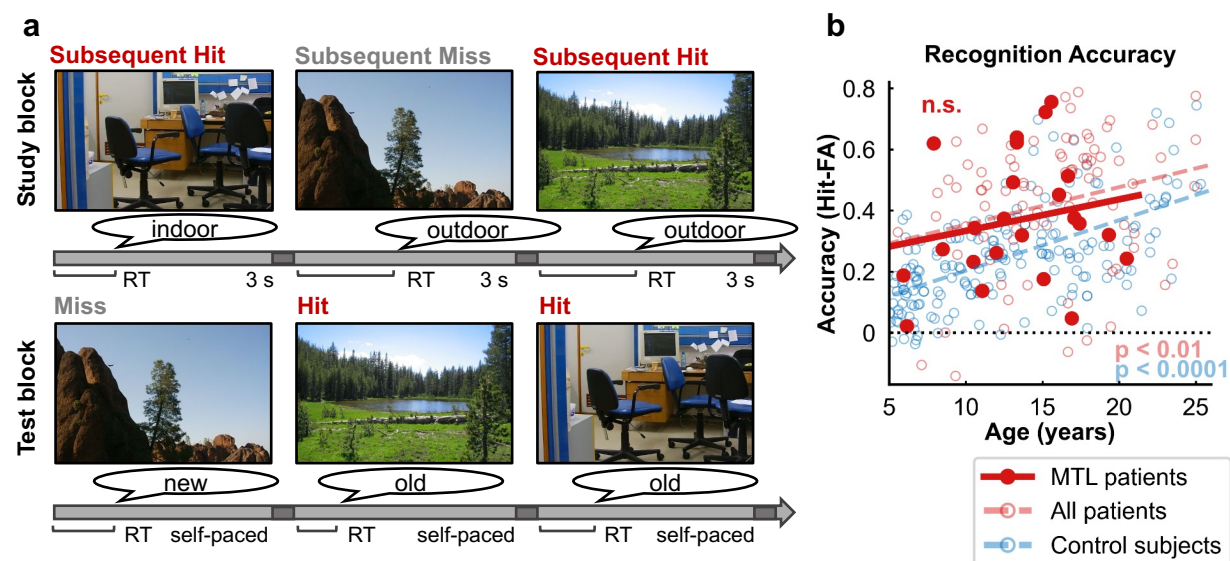
140 the developing brain[63].

141
142 **Figure 1. Scene subsequent memory paradigm and memory performance.**
143 (**a**) Subsequent memory paradigm. Pictures of scenes were presented in two consecutive study-test
144 cycles. In each study cycle, subjects studied 40 scenes (3 s each, separated by a 0.5-s interstimulus
145 fixation) and indicated whether each scene was indoor/outdoor. In each test cycle, subjects were
146 tested on all 40 studied scenes, intermixed with 20 new scenes as foils. Subjects made an old/new
147 judgment of each scene based on whether they remembered seeing the scene at study. The test
148 was self-paced. Each response at the test was coded as a hit (old response to a studied scene),
149 miss (new response to a studied scene), correct rejection (new response to a foil scene), or false
150 alarm (old response to a foil scene). Based on the test response, scenes at the study cycle were
151 categorized as subsequent hit or subsequent miss.
152 (**b**) Recognition accuracy by age. Epilepsy patients with MTL electrode coverage (red filled circle and
153 solid line) demonstrate a similar pattern of age-related increase in recognition accuracy (hit rate –
154 false alarm rate) as all epilepsy patients (red empty circle and dashed line) and normal developing
155 control subjects (blue empty circle and dashed line).

HFA peak latency increases along the MTL posterior-to-anterior axis

HFA has been used to investigate the temporal dynamics of brain activity during cognitive tasks in adults[64–68] and the developing brain[37]. We analyzed ECoG signals from 90 artifact-free and nonpathological surface MTL electrodes [median(IQR), 4(2) electrodes/subject] across 23 subjects. A time-frequency representation of power for each study trial was computed from 70 to 150 Hz across 30 logarithmically spaced frequency bands, z-scored on the pre-stimulus baseline via statistical bootstrapping[37,68] for each frequency band, and then averaged across frequencies. Trials with incorrect indoor/outdoor responses were excluded, partly controlling for the effects of attention during study on memory formation.

We plotted HFA across all MTL electrodes ordered from posterior to anterior (Fig. 2a) and observed that scene viewing induced increased HFA in both subsequent hit and subsequent miss trials (Fig. 2a; $z > 2.75$, $p < 0.01$). Moreover, the temporal dynamics of HFA differed between posterior and anterior electrodes. In posterior electrodes, HFA increased after scene onset and persisted throughout the first second of scene viewing (Fig. 2a). In anterior electrodes, HFA increased later during scene presentation (Fig. 2a). Spatiotemporal dynamics along the posterior-to-anterior axis were quantified with the correlation between HFA peak latencies and the y-coordinates of electrodes. Here, HFA peak latency was defined as the time of maximum HFA between scene onset and 0.2 s after scene category response onset on each trial (see Fig. 2b for examples) and averaged across trials. A linear mixed-effects model with subsequent memory (i.e., hit vs. miss) and y-coordinate as fixed effects, and subjects and nested electrodes as random effects revealed a main effect of y-coordinate ($\beta = 0.66$, $t(176) = 3.24$, $p = 1.4 \times$

8

179   10^{-3}) and subsequent memory $\times$ y-coordinate interaction (β = -0.31, t(176) = -2.45, p =

180   0.02). No main subsequent memory effect was observed (β = 0.10, t(176) = 0.76, p =

181   0.44). Post-hoc analysis using separate linear mixed-effect models for subsequent hit

182   and miss trials, with y-coordinate as the fixed effect and subjects and nested electrodes

183   as random effects, revealed that HFA peak latency increased from posterior to anterior

184   along the MTL long axis in subsequent hit (Fig. 2c, left; β = 0.31, t(88) = 4.44, p = 2.59 $\times$

185   10^{-5}) but not in subsequent miss trials (Fig. 2c, right; β = 0.07, t(88) = 0.61, p = 0.55).

186   The different posterior and anterior HFA patterns (Fig. 2a) and increased HFA peak

187   latency from posterior to anterior (Fig. 2b) support different processes along the MTL

188   long axis. We thus continued to investigate functional differentiation along the MTL long

189   axis in the developing brain by defining posterior and anterior MTL regions based on the

190   localization of MTL electrodes across subjects. We classified MTL electrodes as

191   posterior or anterior using the midpoint between the most anterior and most posterior

192   electrodes (Fig. 2d, y = -14.35 mm). This approach allowed utilizing the extant data and

193   avoids potential biases in defining functional subregions along the MTL long axis[22,23,26].

194   Posterior MTL activity was sampled from 29 electrodes [median(IQR), 1(1)

195   electrodes/subject] across 17 subjects (13.25 ± 3.68 years), and anterior MTL activity

196   was sampled from 61 electrodes [median(IQR), 3(2) electrodes/subject] across 20
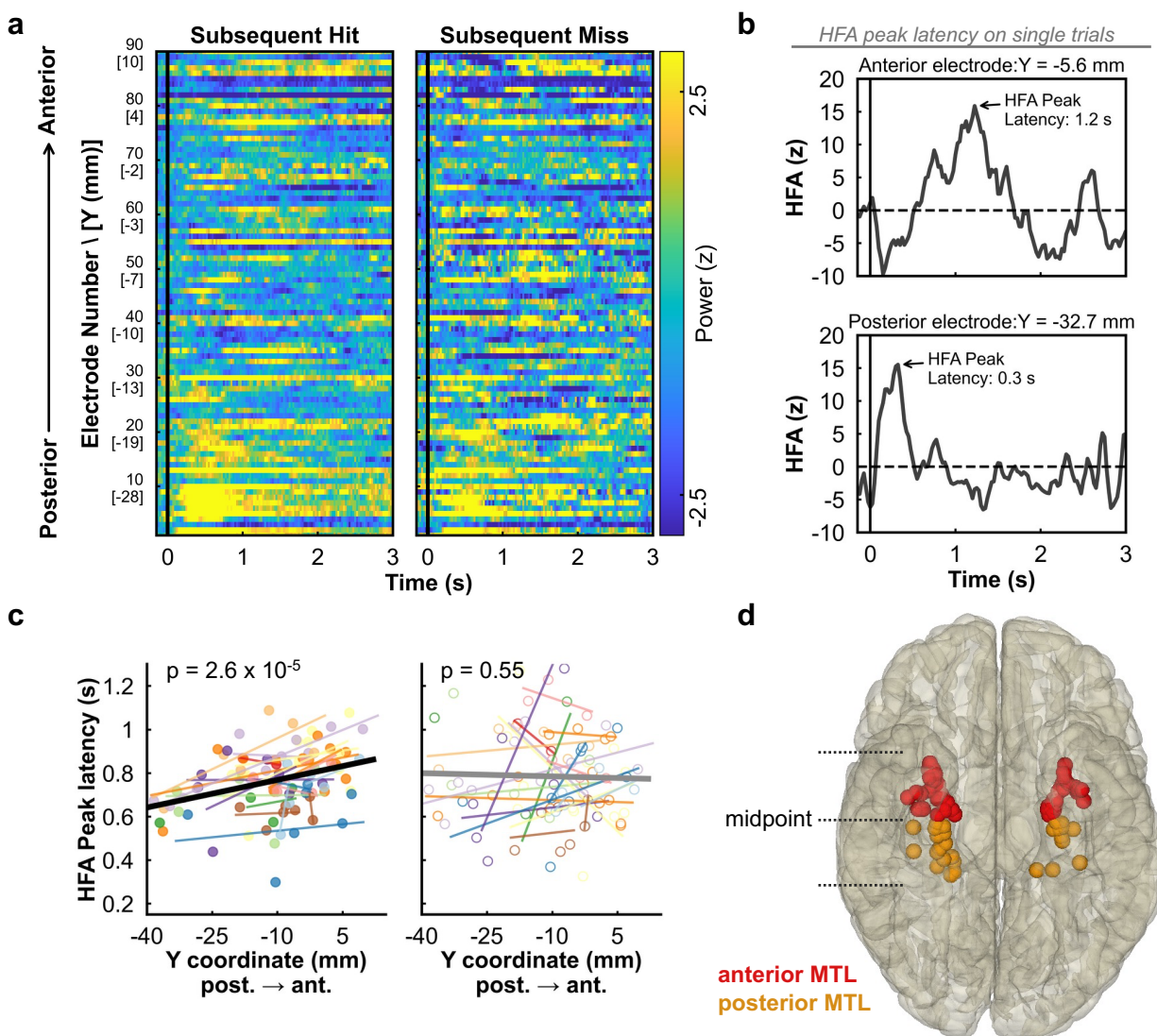
197   subjects (12.98 ± 3.88 years).

198

199
200 **Figure 2. Spatiotemporal dynamics of HFA along the MTL long axis.**
201 (**a**) HFA across all MTL electrodes sorted by y-coordinates, ordered from posterior to anterior. The
202 solid vertical line indicates scene onset. Scene viewing induced increased HFA (z > 2.57, p < 0.01)
203 in the MTL in both subsequent hit (left) and miss trials (right). The HFA increases occurred in the first
204 second of scene viewing in posterior electrodes but were present later during the scene presentation
205 in anterior electrodes.
206 (**b**) Example trials showing HFA peak latency definition from an anterior (top) and a posterior
207 (bottom) electrode.
208 (**c**) HFA peak latency increased along the MTL long axis in subsequent hit trials (left) but not in
209 subsequent miss trials (right). Each color represents a single subject.
210 (**d**) Electrode coverage of the posterior and anterior MTL from all subjects. Electrodes were
211 classified as posterior or anterior using the midpoint between the most anterior and most posterior
212 electrodes. Orange, posterior MTL; red, anterior MTL.

213 **HFA in the anterior MTL tracks scene category response**

10

214   We next examined the temporal dynamics of HFA relative to scene onset and scene

215   category responses (i.e., indoor/outdoor) in the posterior and anterior MTL. We first

216   visualized HFA on the single-trial level by averaging across electrodes within each

217   region per subject, pooling trials across all subjects, and sorting them by response time

218   (RT). We observed that HFA in the posterior MTL increased after stimulus onset and

219   was sustained throughout the first second of scene viewing regardless of RT in

220   subsequent hit trials (Fig. 3a). In contrast, HFA in the anterior MTL did not increase

221   following stimulus onset but instead increased around each trial's RT in both

222   subsequent hit and miss trials (Fig. 3b). HFA peak latency was again used to assess the

223   relationship between HFA and RT. A linear mixed-effects model with region (posterior

224   MTL vs. anterior MTL), subsequent memory (hit vs. miss), and RT as fixed effects, and

225   subjects and nested electrodes as random effects, revealed a significant region $\times$ RT

226   interaction (β = -0.41, t(172) = -2.08, p = 0.04) and region $\times$ RT $\times$ subsequent memory

227   interaction (β = 0.27, t(172) = 2.22, p = 0.03). There was no significant region,

228   subsequent memory, RT, region $\times$ subsequent memory, or subsequent memory $\times$ RT

229   effects (Table S2).

230   Post hoc analyses were conducted with per-region linear mixed-effects models with

231   subsequent memory and RT as fixed effects. In the posterior MTL, there were no

232   significant subsequent memory or RT effects on HFA peak latency (Table S3). However,

233   we observed a significant subsequent memory $\times$ RT interaction (Fig. 3c; β = 0.48, t(54)

234   = 3.32, p = 1.6×10^{-3}), with HFA peak latency tracking RT in subsequent miss (β = 0.69,

235   t(27) = 4.85, p = 4.5×10^{-5}) but not subsequent hit (β = 0.21, t(27) = 1.74, p = 0.09) trials,

236   suggesting scene onset-induced activity rather than response-related activity in the

11

237 posterior MTL is beneficial for successful memory formation. In the anterior MTL, we

238 observed a significant RT effect (Fig. 3d; $\beta = 0.74$, $t(118) = 3.04$, $p = 2.9 \times 10^{-3}$) in that

239 the anterior MTL HFA tracked subjects' scene category responses. We did not observe

240 significant subsequent memory or subsequent memory $\times$ RT interaction effects (Table

241 S3). These findings suggest an endogenous process in the anterior MTL, likely

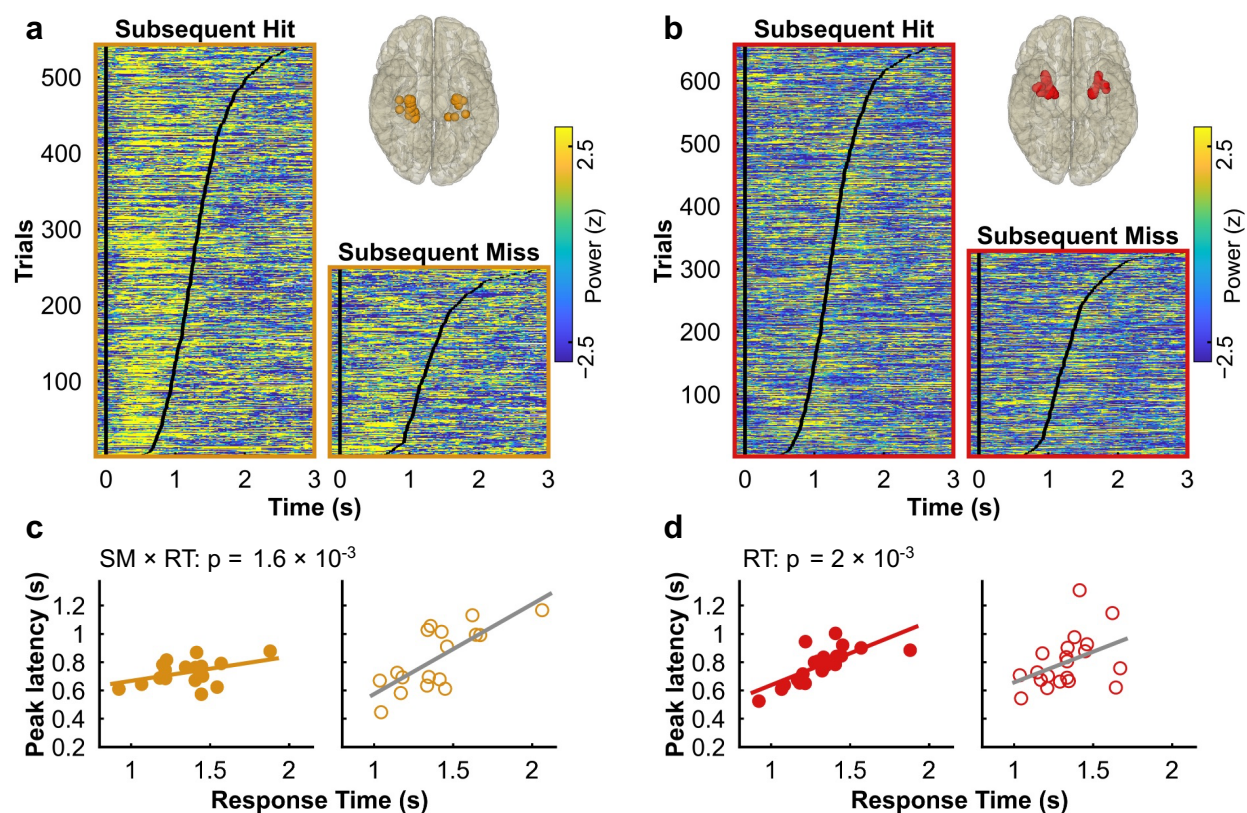242 reflecting conceptual category representation of visual scenes.

243
244 **Figure 3. Associations of HFA peak latency with scene category RT.**
245 (**a**) HFA across all trials in the posterior MTL, sorted by RT (black tick marks) from the fastest to
246 slowest response trial in subsequent hit (left) and miss trials (right). Each trial represents data
247 averaged across electrodes within the posterior MTL per subject. The solid vertical line indicates the
248 scene onset.
249 (**b**) Same as (a) in the anterior MTL.
250 (**c**) HFA peak latency in the posterior MTL was not associated with RT in hit trials (left) but showed a
251 positive association in subsequent miss trials (right). P-value indicates subsequent memory $\times$ RT
252 interaction.
253 (**d**) HFA peak latency in the anterior MTL positively associated with RT in both subsequent hit (left)
254 and miss (right) trials. P-value indicates the main effect of RT.

12

HFA in the posterior MTL predicts memory formation and is associated with recognition accuracy

After identifying different temporal dynamics of activity in the posterior and anterior MTL, we further investigated the subsequent memory effects (SMEs) by contrasting the HFA of subsequent hit trials with subsequent miss trials. We analyzed SMEs by aligning the trials to scene onset for scene-induced SMEs and by aligning the trials to subjects' scene category response onset for response-related SMEs. SMEs were analyzed between -0.15 to 1 s for stimulus-locked data and between -1 to 0.2 s for response-locked data. We conducted each subsequent memory analysis with a linear mixed-effects model with subsequent memory (hit vs. miss) as the fixed effect and subjects and nested electrodes as random effects and used cluster-based correction for multiple comparisons. In the posterior MTL, we observed increased HFA during successful memory formation in both stimulus-locked data (i.e., positive SMEs, 0.475 to 0.625 s, p = 0.03; Fig. 4a, top) and response-locked data (-0.475 to -0.375 s, p = 0.04, Fig. 4a, bottom). These findings provide evidence that posterior MTL HFA is beneficial for successful memory formation of visual scenes. In the anterior MTL, we observed clusters of positive SMEs in both stimulus-locked data (0.650 to 0.775 s, p = 0.02; Fig. 4b, top) and response-locked data (-0.425 to -0.275 s, p = 8 $\times$ 10^{-3}; Fig. 4b, bottom). Of note, these positive SMEs in the anterior MTL were driven by decreased HFA in subsequent miss trials.

We then examined whether the observed SMEs were associated with memory performance or age. We averaged across time points within each cluster of SMEs per subject and submitted the averaged data into multiple regression with recognition accuracy and age as predictors. In the posterior MTL, scene-induced SME was not

13

279   associated with recognition accuracy or age (Fig. 4c, top; Table S4). However,

280   response-locked SME was positively associated with recognition accuracy (Fig. 4c,

281   bottom; $\beta = 0.56$, $t(13) = 2.57$, $p = 0.02$). We observed no age or age $\times$ recognition

282   accuracy interaction effects for response-locked SME (Table S4), demonstrating that

283   HFA in the posterior MTL supports memory independent of age. In the anterior MTL, we

284   did not observe recognition accuracy, age, or age $\times$ recognition accuracy interaction

285   effects on either scene-induced or response-related SMEs (Fig. 4d; Table S4). Taken

286   together, our findings demonstrate that the posterior MTL supports scene processing

287   across age, with HFA serving as a neurophysiological feature linked to memory

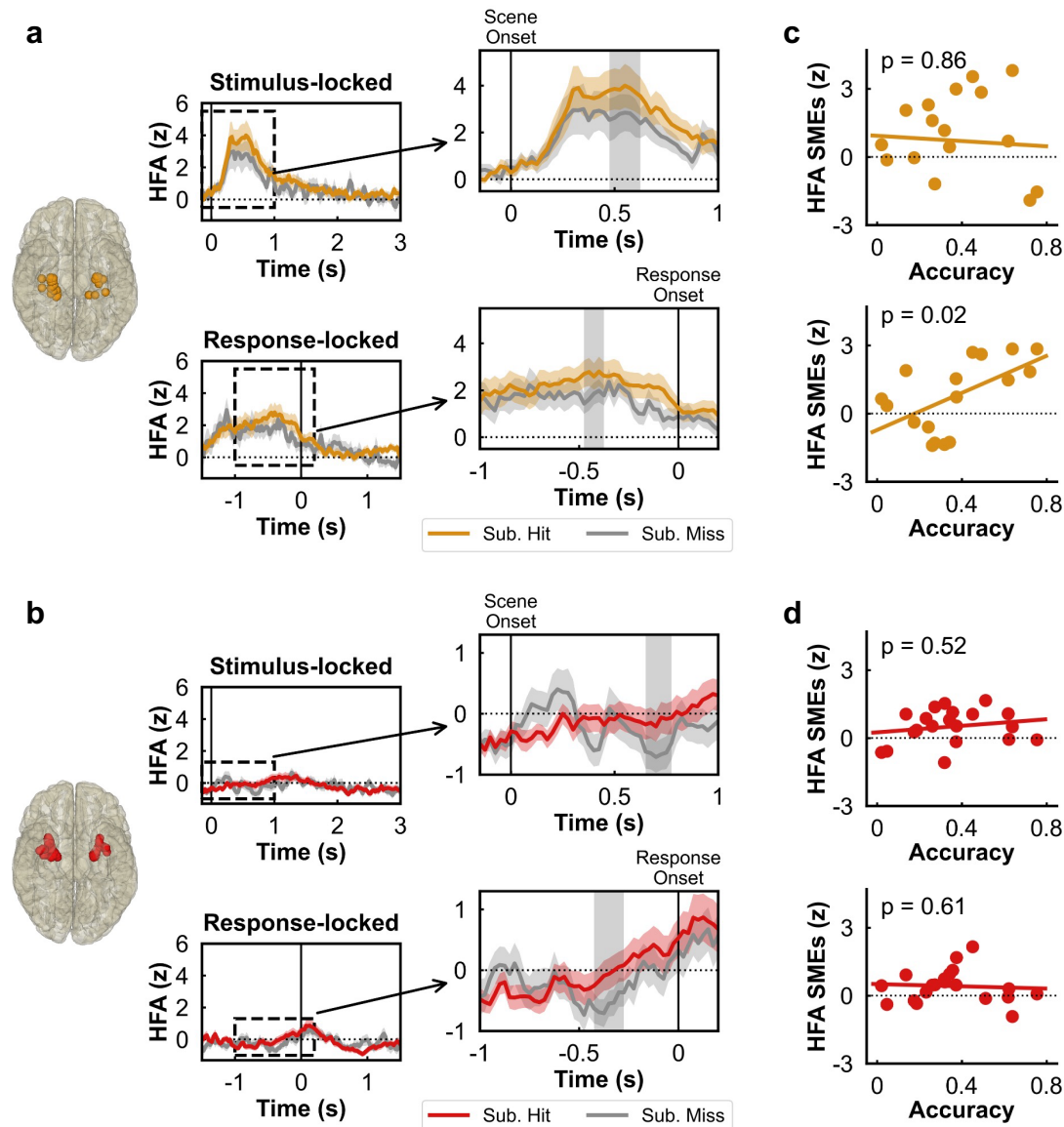288   formation of visual scenes.

14

Figure 4. HFA signatures of successful memory formation.
(**a**) HFA SMEs in the posterior MTL. Top: HFA locked to scene onset. The solid vertical line indicates the scene onset. The inset on the right zooms in on the first second after scene onset, indicating the time window for which SMEs were analyzed. Bottom: HFA locked to scene category response onset. The solid vertical line indicates response onset. The inset on the right zooms in on the one second before the response, indicating the time window for which SMEs were analyzed. HFA data were averaged across subjects, and the shaded areas represent the standard error of the mean. The gray shaded area in the insets denotes cluster-corrected significant SMEs. Sub. Hit, subsequent hit; Sub. Miss, subsequent miss.
(**b**) Same as (a) in the anterior MTL.
(**c**) Top: scene-induced SME in the posterior MTL was not associated with recognition accuracy. Bottom: response-related SME in the posterior MTL was positively associated with recognition accuracy. The SMEs are grey shaded area in (a).
(**d**) Scene-induced (top) and response-related (bottom) SMEs were not associated with recognition accuracy. The SMEs are grey-shaded areas in (b).

Theta oscillations in the anterior MTL are associated with recognition accuracy

306   Theta is the predominant oscillation in the MTL and is posited to support MTL

307   computations involved in information integration[55–57]. Emerging evidence suggests that

308   neural oscillations, including theta, show variability in center frequency and power

309   across brain regions[69–71], task states[72,73], and development[36,40,42,63,74–76] and aging[77–79].

310   To characterize theta variability across MTL subregions and individuals, we utilized a

311   widely used oscillation detection algorithm, SpecParam[80], to isolate and parameterize

312   oscillations (see Fig. 5a for an electrode example from the anterior MTL). Neural

313   oscillations are defined as peaks above the 1/f aperiodic component in the power

314   spectrum (Fig. 5a, top), and each peak can be parameterized with measures of center

315   frequency, power, and bandwidth (Fig. 5a, bottom). Oscillation detection was conducted

316   between 1-30 Hz per electrode on the average power spectrum, separately for

317   subsequent hit and miss trials. As shown in Fig. 5b, electrodes in the posterior and

318   anterior MTL exhibited oscillatory peaks in both subsequent hit and miss trials. The

319   frequency distribution of the largest peak, i.e., peak with the largest power, across all

320   electrodes per region was examined to identify the frequency range of the dominant

321   oscillation (Fig. 5c). We observed that the largest peaks clustered between ~1-10 Hz in

322   both the posterior [Fig. 5c; median(IQR): subsequent hit, 7.59(7.67) Hz; subsequent

323   miss, 7.61(2.23) Hz] and anterior MTL [Fig. 5c; median(IQR): subsequent hit, 6.93(6.14)

324   Hz; subsequent miss: 7.11(6.78) Hz], confirming that theta oscillations dominate the

325   developing MTL[36]. We selected the largest peak between 1-10 Hz as theta oscillation

326   per electrode based on the frequency distribution for further analysis.

327   We examined whether theta parameters (i.e., frequency, power, and bandwidth, see

328   Fig. 5a) differed between the posterior and anterior MTL and between subsequent hit

16

329   and miss trials. Linear mixed-effects models were used per parameter with region

330   (posterior MTL vs. anterior MTL) and subsequent memory (hit vs. miss) as fixed effects

331   and subjects and nested electrodes as random effects. Theta frequency did not differ

332   between regions or between subsequent hit and miss trials (see Fig. S1; Table S5).

333   However, we observed a significant negative SME on theta power (Fig. 5d; β = -0.11,

334   t(175) = -2.95, p = 3.7 $\times$ 10^{-3}), extending previous findings of broadband power

335   decreases during successful memory formation[36,42] to narrowband theta oscillations. No

336   significant region or region $\times$ subsequent memory effect was observed on theta power

337   (Fig. 5d; Table S5). Theta bandwidth also did not differ between regions or between

338   subsequent hit and miss trials (Fig. S1; Table S5). The lack of regional differences

339   across parameters is consistent with the idea that a common theta frequency may

340   provide a functional basis for the interaction and information transformation between

341   these two regions[71,81].

342   We then examined individual differences. Each theta parameter was submitted to a

343   linear mixed-effects model per region with age, recognition accuracy, and subsequent

344   memory as fixed effects, and subjects and nested electrodes as random effects. In the

345   posterior MTL, no significant effects were observed on theta frequency (see Fig. S2a;

346   Table S6). However, we observed significant effects of age and subsequent memory on

347   theta power (Fig. 5e; age: β = 0.47, t(50) = 2.15, p = 0.04; subsequent memory: β = -

348   0.12, t(50) = -3.12, p = 3.0 $\times$ 10^{-3}). No other significant effects were observed for theta

349   power (see Fig. S2a; Table S6), and no significant effects were observed for theta

350   bandwidth (see Fig. S2a; Table S6). Taken together, we found that, in the posterior MTL,

351 theta power increased with age, possibly reflecting the reduced involvement of theta

352 with development.

353   In the anterior MTL, we observed that higher theta frequency was associated with

354 better memory performance (Fig. 5f; $\beta = 0.42$, $t(113) = 2.77$, $p = 6.6 \times 10^{-3}$). No other

355 significant effects on theta frequency were observed (see Fig. S2b; Table S7). For

356 power, we observed a significant SME ($\beta = -0.11$, $t(113) = -3.00$, $p = 3.3 \times 10^{-3}$). No

357 other significant effects were observed for power (see Fig. S2b; Table S7), and no

358 significant effects were observed for theta bandwidth (see Fig. S2b; Table S7). Taken

359 together, we found that, in the anterior MTL, faster theta oscillations were associated

360 with better memory performance independent of age, suggesting increased precision of

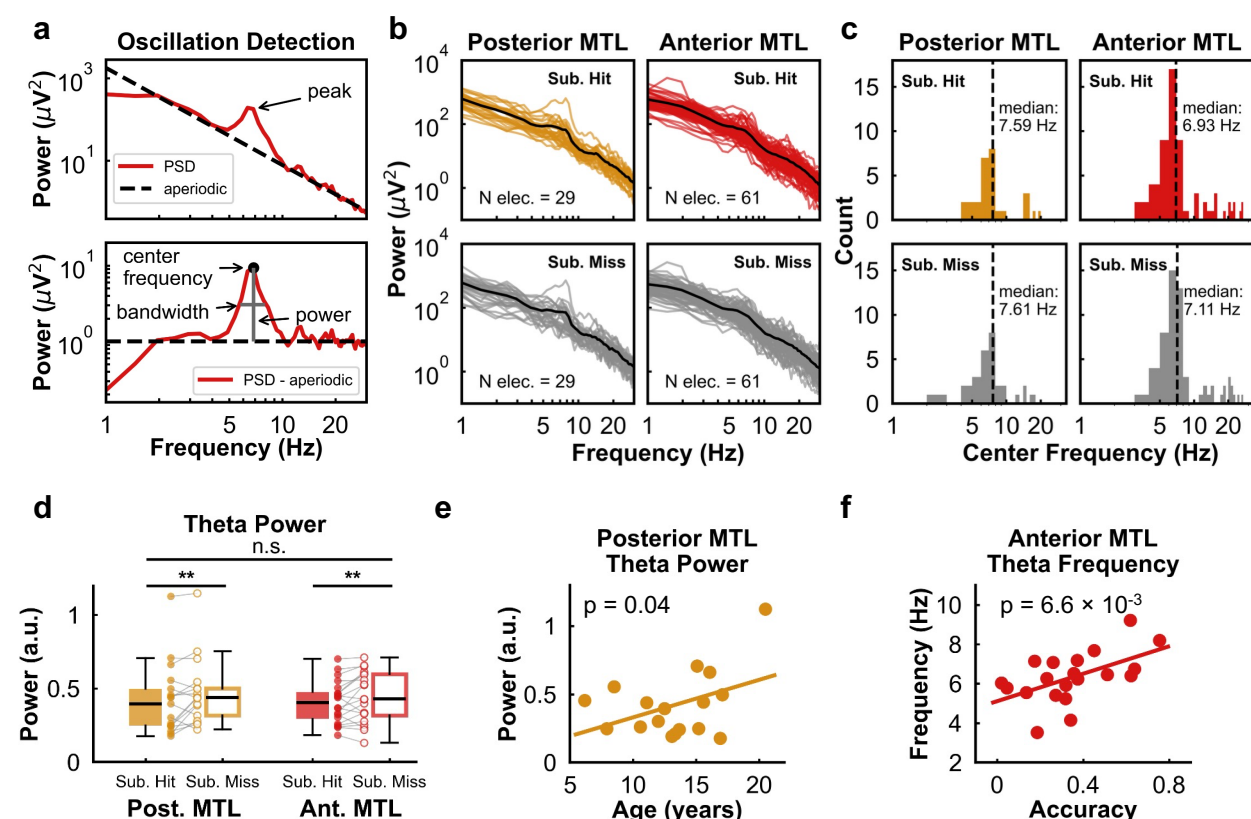361 activity may support better memory in the developing brain[42].

362

18

363 **Figure 5. Characterizing theta oscillations in the posterior and anterior MTL.**
364 (**a**) Top: power spectrum of one representative electrode from the anterior MTL showing the
365 existence of an oscillation as a peak over the estimated aperiodic activity (black dashed line).
366 Bottom: power spectrum after subtracting the estimated aperiodic activity. The detected oscillation is
367 parametrized with center frequency, power, and bandwidth.
368 (**b**) Power spectra across all electrodes for subsequent hit (top) and miss (bottom) trials. The black
369 line in each plot indicates the averaged power spectrum across all electrodes within each region.
370 Sub. Hit, subsequent hit; Sub. Miss, subsequent miss.
371 (**c**) Center frequency distribution of the largest peak between 1-30 Hz shows that theta dominates
372 the MTL.
373 (**d**) Theta power between regions and between subsequent hit and miss trials. ** $p \leq 0.01$. Post.
374 MTL, posterior MTL; Ant. MTL, anterior MTL.
375 (**e**) Posterior MTL theta power increased with age.
376 (**f**) Anterior MTL theta frequency was positively associated with recognition accuracy.

Anterior MTL theta-HFA coupling before scene category response predicts memory formation

379   The association of theta oscillations with memory performance suggests that theta-

380 related mechanisms underlie memory. We next examined theta-HFA phase-amplitude

381 coupling, a mechanism that has been posited to support information binding and

382 mnemonic representations[55–58]. Examining theta-filtered and HFA-filtered signals on the

383 single-trial level (see Figs. 6a, 6b for examples), we observed theta phase-dependent

384 variations in HFA, and the dependence varied across time. To capture the temporal

385 dynamics of theta-HFA coupling, we analyzed event-related theta-HFA PAC (ERPAC).

386 ERPAC was calculated with theta defined by the individually detected frequency per

387 electrode for subsequent hit and miss trials. This approach allows the capture of

388 coupling strength while controlling the inter-individual differences in theta

389 parameters[36,42,80]. Building on the distinct temporal dynamics of the posterior and

390 anterior MTL revealed by HFA, we again investigated SMEs by aligning the studied

391 trials to scene onset for scene-induced effects and scene category response onset for

392 response-related effects. Subsequent memory analysis was conducted using linear

393 mixed-effects model with cluster-based correction. We did not observe any SMEs in the

394 posterior MTL in either stimulus-locked data or response-locked data (Fig. 6c). In the

19

395   anterior MTL, no SMEs were observed in stimulus-locked data (Fig. 6d, top). However,

396   a cluster of positive SMEs (-0.470 to -0.354 s, p = 0.04; Fig. 6d, bottom) was observed

397   in response-locked data. These positive SMEs suggest that theta-HFA coupling in the

398   anterior MTL, occurring before subjects' scene category responses, underlies

399   conceptual scene category representation and facilitates successful memory formation.

400   After identifying positive SMEs in the anterior MTL, we examined whether this

401   signature of memory formation was associated with age or recognition accuracy. We

402   averaged across time points within this cluster of positive SMEs (Fig. 6d, bottom) per

403   subject and submitted the averaged ERPAC into multiple regression with recognition

404   accuracy and age as predictors. We did not observe any significant effects of age or

405   recognition accuracy (Table S8). Controlling for individual differences in theta

406   parameters, the lack of individual differences in ERPAC indicates that theta frequency

407   (see Fig. 5f), but not the strength of theta-HFA coupling, explains individual differences

408   in recognition accuracy, suggesting that increased precision of the coupling mechanism

409   supports better memory in the developing brain[42].

410   Lastly, theta supports memory by operating through distinct theta phases[82–84]. To

411   capture the theta phase associated with increased HFA in the anterior MTL, we

412   analyzed the preferred phase of HFA during the time window of significant SMEs (see

413   Fig. 6d, bottom). Theta phases were divided into 18 bins from $-\pi$ to π, and HFA was

414   binned based on the theta phases. We observed increased HFA at the theta trough

415   during subsequent hit trials (Figs. 6e, 6f). In contrast, during subsequent miss trials,

416   HFA increased at both the trough and midpoint. Together, these observations suggest

20

417   that theta trough at the anterior MTL provides the optimal cyclical window for neuronal

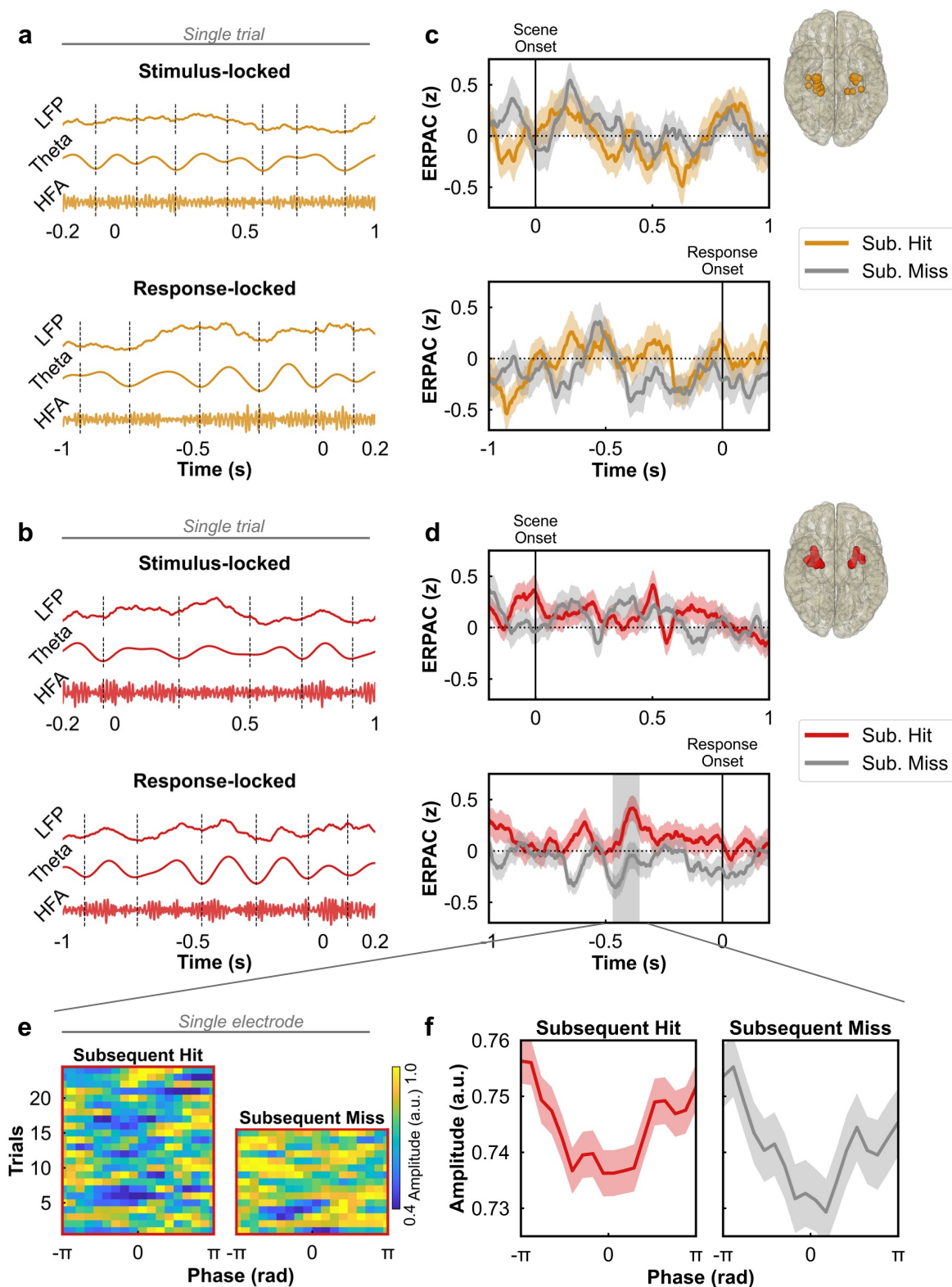418   activity and underlies successful memory formation.

Figure 6. Anterior MTL theta-HFA coupling associated with successful memory formation.
(**a**) Raw, theta-filtered, and HFA-filtered signals of a representative subsequent hit trial from a posterior MTL electrode for stimulus-locked data (top) and response-locked data (bottom). Dashed vertical lines indicate theta troughs.

424   (**b**) Same as (a) from an anterior MTL electrode.

425   (**c**) ERPAC for subsequent hit and miss trials across all subjects in the posterior MTL. Top: ERPAC

426   locked to stimulus onset. The solid line at time zero indicates stimulus onset. Bottom: ERPAC locked

427   to response onset. The solid line at time zero indicates "indoor/outdoor" response onset. Shaded

428   areas represent the standard error of the mean across subjects. No significant SMEs were observed

429   in the posterior MTL. Sub. Hit, subsequent hit; Sub. Miss, subsequent miss.

430   (**d**) Same as (c) for the anterior MTL. A cluster of positive SMEs was observed preceding response

431   onset (bottom). The gray shaded area denotes cluster-corrected significant SMEs.

432   (**e**) HFA from the time window of significant SMEs (Fig. 6d, bottom) binned by theta phases across

433   subsequent hit (left) and miss trials (right) from a representative anterior MTL electrode.

434   (**f**) HFA from the time window of significant SMEs (Fig. 6d, bottom) binned by theta phases across all

435   subjects for subsequent hit (left) and miss trials (right). Shaded areas indicate the standard error of

436   the mean across subjects.

437   **Posterior-anterior MTL theta phase coupling predicts memory formation**

438   Having identified distinct neurophysiological features underlying memory formation

439   in the posterior and anterior MTL, we last sought to examine the interaction between

440   these two subregions. Oscillation phase coupling is posited as a mechanism to support

441   inter-regional interaction and information transfer[59,62]. The consistency in theta

442   parameters between the posterior and anterior MTL (See Fig. 5d, Fig. S1) may provide

443   a functional basis for their interaction. Theta phases between the posterior and anterior

444   MTL were aligned during single trials (Fig. 7a), and the phase-locking value (PLV; Fig.

445   7b) was analyzed to measure theta phase coupling between these two regions. Here,

446   PLV was calculated with the individually detected theta frequency per electrode for

447   subsequent hit and miss trials. SMEs were analyzed using linear mixed-effects models

448   with subsequent memory (hit vs. miss) as the fixed effect and subjects and nested

449   electrodes as random effects. We observed two clusters of positive SMEs in stimulus-

450   locked data (Fig. 7b, top; cluster 1, -0.200 to 0.144 s from scene onset, $p = 1 \times 10^{-3}$;

451   cluster 2, 0.271 to 1.000 s from scene onset, $p < 1 \times 10^{-3}$) and one cluster of positive

452   SMEs in response-locked data (Fig. 7b, bottom; -0.866 to 0.200 s from scene category

453   response onset, $p < 1 \times 10^{-3}$), showing that sustained interaction between the posterior

454   and anterior MTL supports successful memory formation.

23

455   We then examined whether any of these SMEs were associated with age or

456   recognition accuracy. The average SMEs per subject for each cluster were submitted to

457   multiple regression with accuracy and age as predictors. We did not observe any

458   significant effects for stimulus-locked or response-related SMEs (Table S9). Controlling

459   for individual differences in theta frequency, these findings indicate that increased

460   precision (see Fig. 5f), rather than the strength, of inter-regional theta coupling is

461   associated with better memory performance[42].

462   Lastly, we examined whether posterior MTL HFA were coupled to anterior MTL theta

463   phase at the individually defined frequency. We analyzed inter-regional theta-HFA

464   coupling with ERPAC. Linear mixed-effects models revealed no significant SMEs in

465   either stimulus- or response-locked data (see Fig. S3). However, in the exploratory

466   analysis of examining the correlation between posterior MTL HFA and anterior MTL

467   theta, we observed significant correlations. Posterior MTL HFA during the stimulus-

468   locked SMEs time window (see Fig. 4a, top) was positively correlated with anterior MTL

469   theta frequency in both subsequently hit and miss trials (Fig. 7c, left; hit, $r = 0.68$, $r = 6.8$

470    $\times 10^{-3}$; miss, $r = 0.65$, $p = 0.01$). During the response-locked SMEs time window (see

471   Fig. 4a, bottom), posterior MTL HFA was positively correlated with anterior MTL theta

472   frequency in subsequent hit trials (Fig. 7c, right; $r = 0.60$, $p = 0.02$), but not in miss trials

473   (Fig. 7c, bottom; $r = 0.36$, $p = 0.21$). No other correlations between posterior MTL HFA

474   and anterior MTL theta parameters were observed (see Figure S4; Table S10). Taken

475   together, these findings suggest that inter-regional theta coupling facilitates the transfer

476   of information and supports the representation of both the details and the conceptual

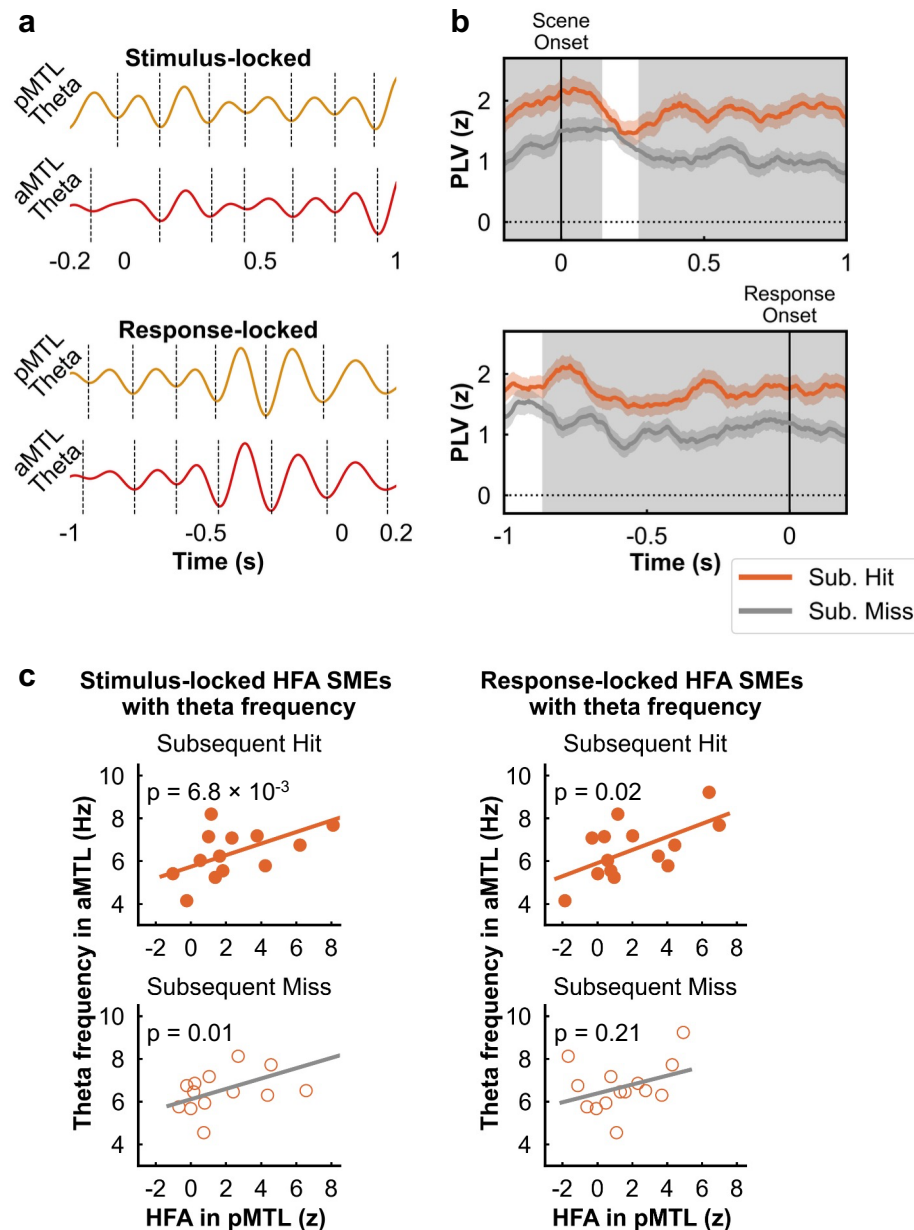477   category of visual scenes during memory formation.

Figure 7. Theta coupling associated with successful memory formation.
(**a**) Top: theta-filtered signal of a representative subsequent hit trial from a posterior (top) and anterior (bottom) MTL electrode for stimulus-locked data. Bottom: The same signal locked to the scene category response onset. Dashed vertical lines indicate theta troughs.
(**b**) Posterior-anterior MTL theta coupling in stimulus-locked (top) and response-locked (bottom) data. Shaded areas represent the standard error of the mean across subjects. The gray shaded areas denote cluster-corrected significant SMEs. Sub. Hit, subsequent hit; Sub. Miss, subsequent miss.
(**c**) Correlation of posterior MTL HFA with anterior theta frequency for subsequent hit (top) and miss (bottom) trials. Left: HFA from the time window of significant SMEs from stimulus-locked data, see Fig. 4a, top, grey shaded area. Right: HFA from the time window of significant SMEs from response-locked data, see Fig. 4a, bottom, grey shaded area.

DISCUSSION

Human episodic memory is a multifaceted construct that relies on the representations of both perceptual and conceptual information about experiences[85–87]. Utilizing the high spatiotemporal precision afforded by ECoG, we investigated how the developing MTL supports memory formation for visual scenes. We focused our investigation on identifying features that correspond to representations of perceptual details and conceptual category of visual scenes during memory formation, defined by their timing relative to the scene onset and categorization response. Distinct neurophysiological features were observed in the posterior and anterior MTL, suggesting complementary representations of perceptual and conceptual information during memory formation in the developing MTL.

HFA peak latency indicates different processes in the posterior and anterior MTL

Leveraging the high spatiotemporal resolution of HFA, we observed that HFA peak latency increased along the posterior-to-anterior axis during subsequent hit but not miss trials, suggesting information transfer along the MTL long axis during successful memory formation. Early posterior activity likely reflects responses to visual scenes[9,22,23], whereas later anterior activity supports the posited role of the anterior region in integrating incoming visuospatial information for higher-level representations[8,15,27–29]. To test whether these dynamics tracked scene onset or scene category responses (i.e., indoor/outdoor), we divided the MTL into posterior and anterior regions. In the posterior MTL, scene onset induced HFA increases at the single-trial level during subsequent hit but not miss trials (Fig. 3a). Moreover, HFA peak latency

26

514   during subsequent miss but not hit trials correlated with subjects' RTs. These findings

515   suggest that scene-induced posterior MTL HFA supports successful memory formation.

516   By contrast, in the anterior MTL, HFA peaked around subjects' scene category

517   responses at the single-trial level (Fig. 3b), and peak latencies correlated with subjects'

518   RTs. This category response-related activity supports the idea that the anterior MTL is

519   involved in the conceptual category representations of visual scenes[8,15,27–29]. Notably,

520   anterior MTL HFA tracked scene category responses in both subsequent hit and miss

521   trials, indicating that while it reflects category processing, it may not be the primary

522   feature supporting memory formation in the anterior MTL. These latency findings

523   support the hierarchical processing along visual pathways[88–90], in which perceptual

524   details are represented earlier in more posterior regions and stimulus identity

525   representations are formed over time in anterior regions.

Posterior MTL HFA and memory

526

527   Extending the widely observed preferential memory responses to visual scenes in

528   the posterior MTL in fMRI studies[9,22,23,33,34], we observed increased HFA in subsequent

529   hit trials (i.e., positive subsequent memory effects) after scene onset and before

530   subjects' scene category responses. In addition, increased HFA before subjects' scene

531   category responses was positively associated with memory performance, underscoring

532   HFA as a neurophysiological feature of the posterior MTL supporting memory. In the

533   anterior MTL, we observed positive HFA subsequent memory effects after scene onset

534   and before scene category responses. However, unlike the pronounced HFA increases

535   in the posterior MTL, the anterior MTL exhibited an overall reduced level of HFA and

536   neither of the subsequent memory effects clusters was associated with memory

537   performance. The reduced level of HFA in the anterior MTL might be due to a smaller

538   number of neurons coding conceptual information[90,91]. Future studies incorporating

539   human single-neuron recordings are needed to investigate the neural computation

540   underlying conceptual representation in the anterior MTL[90,92].

Anterior MTL theta oscillation and memory

542   By systemically detecting and parameterizing neural oscillations in the posterior and

543   anterior MTL, we confirmed that theta oscillations, ranging from ~2-10 Hz, dominate the

544   developing MTL and exhibit significant inter-individual variability. This observation

545   supports the use of individually identified theta oscillations, rather than the canonical

546   broadband theta range (~4-8 Hz), to accurately assess individual differences in neural

547   oscillations and their functional roles[36,80]. After parameterizing theta oscillations by

548   center frequency, power, and bandwidth, we examined the differences in these

549   parameters between subsequent hit and miss trials and the posterior and anterior MTL.

550   Except for theta power differences between subsequent hit and miss trials, theta

551   parameters did not differ in relation to subsequent memory outcome.

552   We observed theta power decreases in subsequent hit trials in both the posterior

553   and anterior MTL, consistent with known broadband low-frequency power decreases

554   during successful memory formation[36,40] and extending the idea of cortical

555   desynchronization in the service of information representation for successful memory[93]

556   to individually detected narrowband low-frequency oscillations. The lack of subsequent

557   memory effects in theta frequency and bandwidth implies that theta oscillations provide

558   an infrastructure for memory processes[36], with the difference between successful and

559   unsuccessful memory formation lying in theta-associated mechanisms, rather than in

560   the oscillations themselves.

561   Although no regional differences in theta parameters were observed, the posterior

562   and anterior MTL differed in how theta parameters were associated with memory

563   performance and age. In the anterior MTL, we observed that faster theta frequency was

564   associated with better memory performance. In line with the correlation between theta

565   frequency and spatial navigation speed in the hippocampus[94,95], increased frequency

566   may underlie increased information processing[40,96], potentially due to faster fluctuations

567   between neuronal excitation and inhabitation[58]. Future studies that detect and

568   parameterize theta during different cognitive tasks, as well as employ computational

569   models, are needed to further elucidate the underlying mechanisms linking theta

570   frequency to cognitive performance. In the posterior MTL, we observed an age-related

571   increase in theta power. Because cortical theta power decreases are associated with

572   memory, the age-related increase in theta power may not be related to memory and

573   rather reflect aspects of posterior MTL development[33,35] that can be elucidated in further

574   research.

Theta-HFA coupling in the anterior MTL supports memory

576   Theta oscillations are posited to underlie memory by facilitating information

577   integration[55–58]. Based on the temporal relationship between neuronal spiking and

578   ongoing theta oscillations in the rodent hippocampus[97], theta is posited to organize

579   neuronal spiking and, by extension, gamma activity or HFA representing information

580   within each cycle[55–58]. In line with the hypothesized functional role of theta, we observed

581   increased theta-HFA coupling in the anterior MTL during successful memory formation,

29

582   extending the theta-gamma code in the hippocampus[98,99] and neocortex[100] to theta-HFA

583   coupling in the MTL cortex. This memory-related theta-HFA coupling occurred before

584   subjects' scene category responses, indicating that conceptual category representation

585   in the anterior MTL may be supported through the integration of visual information

586   facilitated by theta-HFA coupling. The theta-HFA coupling subsequent memory effects

587   were not associated with individual differences in memory performance. This is in

588   contrast to theta frequency in the anterior MTL, which was related to individual

589   differences in memory performance, raising the possibility that faster theta serves as a

590   more finely tuned mechanism supporting memory[36,42] and that its specific frequency is

591   more relevant to memory outcome than theta-HFA coupling strength.

Posterior-anterior theta coupling supports memory

593   Theta oscillations underlie information transfer between brain regions via phase

594   coupling[59,61,62]. Consistent with previous findings of increased inter-regional theta

595   coupling during successful memory formation[36,101,102], we observed increased posterior-

596   anterior MTL theta phase coupling during successful memory formation, likely indicating

597   information transfer between the posterior and anterior MTL. We further explored the

598   interaction between the posterior and anterior MTL by examining the inter-regional

599   cross-frequency phase-amplitude coupling, an inter-regional interaction mechanism that

600   has been reported within hippocampal subfields and between hippocampus and extra-

601   hippocampal cortex in support of memory formation[82,84,103,104]. Specifically, we examined

602   whether posterior MTL HFA, which we identified as relevant to memory, is coupled to

603   anterior MTL theta, which we also identified as relevant to memory. We did not observe

604   anterior-posterior theta-HFA coupling subsequent memory effects in either stimulus-

30

605   locked or response-locked data (see Fig. S3), suggesting that distinct, rather than

606   directly coupled, neurophysiological features support memory along the MTL long axis.

607   However, because of the theta coupling between the posterior and anterior MTL, we

608   further explored the relationship between posterior MTL HFA and anterior MTL theta by

609   directly correlating these measures. We observed that increased posterior HFA was

610   associated with increased anterior theta frequency. Moreover, this positive correlation

611   was specific to subsequent hit but not miss trials for response-related posterior HFA

612   subsequent memory effects (Fig. 7c, right). Posterior MTL HFA was not correlated with

613   other anterior theta parameters (i.e., power, bandwidth; see Fig. S4), suggesting a

614   selective relationship between posterior MTL HFA and anterior MTL theta frequency.

615   These findings indicate increased information transfer and processing along the MTL

616   long axis in support of memory, and that posterior-anterior theta coupling may link

617   distinct neurophysiological features across regions to support the multifaceted

618   representations of visual scenes.

619   **Age-invariant neurophysiological features in the posterior and anterior MTL**

620   Similar to the content-specific organization of the MTL long axis in adults[7–9,22–27], the

621   observed distinct activity latencies and neurophysiological features suggest different

622   representations along the long axis of the developing MTL. Moreover, consistent with

623   age-invariant memory-related activation reported in fMRI studies[31,32], memory-related

624   effects across the examined neurophysiological features in either the posterior or

625   anterior MTL did not differ by age. The similarity of representation patterns to those in

626   adults and the absence of age differences in memory-related neurophysiological

627   features suggest early development of the MTL[3,4,31,105].

31

628   However, some age differences point to ongoing development, particularly of the

629   posterior MTL. The age-related increase in posterior MTL theta power, considered

630   together with subsequent memory theta power decreases, suggests a reduced reliance

631   on theta oscillations across development. We speculate that this reduced involvement

632   of theta is likely due to the increased specialization of scene perception in the posterior

633   MTL with development[33–35,106].

634   Age invariance in memory-related effects may also reflect task or stimulus

635   characteristics. Subjects were asked to study complex visual scenes presented on the

636   screen for 3 seconds and their memory was probed with a recognition test. This task

637   was selected because it involves simple instructions and minimized demands that

638   greatly differ by age such as reading fluency. Future developmental intracranial EEG

639   studies that employ diverse memory tasks can corroborate the findings across different

640   stimulus categories[34], such as scenes, objects, faces, and words and with various

641   mnemonic difficulty levels[35,106].

642   An important additional consideration when investigating age-related differences in

643   regional brain effects is that development likely manifests as the maturation of

644   connectivity between these regions and other key memory brain regions. Previous

645   studies have shown differential connectivity patterns along the MTL long axis. For

646   example, the posterior MTL primarily connects with the posterior hippocampus and

647   other regions within the default mode network, such as the medial parietal cortex and

648   precuneus, while the anterior MTL primarily connects with the anterior hippocampus,

649   amygdala, and orbitofrontal cortex[8,10–12,107]. Differential connectivity may serve as the

650   infrastructure for functional specialization along the MTL long axis. Future studies

651 investigating the development of connectivity mechanisms are needed to better

652 understand the development of the functional specialization of the MTL.

Limitations and future directions

654 Developmental intracranial EEG offers an unparalleled opportunity to investigate the

655 fundamental mechanisms of brain development underlying cognitive development, as it

656 provides localized and temporally precise measures of brain activity. However, such

657 data are rare, and the small sample sizes typically available for evaluating individual

658 differences[36,37,40] may limit our ability to detect potential developmental variability in

659 neurophysiological features[41,42,63]. This limitation necessitates cautious interpretation of

660 the age-invariant findings. Increasing sample size through multi-site collaboration and

661 data sharing is recommended to overcome the sample size issues in developmental

662 intracranial EEG studies[41,42,63]. We also note that, although the task used to probe

663 memory is suitable for both children and adults and is commonly used in developmental

664 research, it uses only visual scenes and incorporates relatively simple memory

665 demands. Employing a task that directly manipulates content-specific representations,

666 or distinguishes between perceptual and semantic processing, would likely help identify

667 more nuanced effects or differential content representation along the long axis of the

668 developing MTL.

669 We also note that we employed a pragmatic, convenience-based distinction to

670 classify electrodes as belonging either to the anterior or posterior MTL; this approach

671 was largely agnostic to known anatomically defined regions, namely the

672 parahippocampal, entorhinal, and perirhinal cortices. This choice was driven by practical

673 limitations, including the absence of harmonized protocols for segmenting MTL

33

674 subregions, substantial individual variability in anatomical landmarks, and the

675 requirement for high-resolution imaging data[108,109]. We confirmed, however, that the

676 midpoint between the most anterior and most posterior electrodes (y = -14.35 mm) used

677 to classify posterior and anterior MTL electrodes is consistent with previous fMRI

678 studies that separate parahippocampal and perirhinal cortices[11,12]. Nonetheless, we

679 referred to the posterior and anterior MTL, rather than to the parahippocampal and

680 perirhinal cortices, to be consistent with our classification approach. Future studies with

681 high-resolution structural MRI data and manual demarcation of MTL subregions at the

682 individual level[22,26,110–112] can further probe anatomical specificity in the

683 neurophysiological features. Lastly, the data presented in the current study are from

684 surface electrodes located on the MTL cortex. The hippocampus exhibits a

685 representation gradient along its long axis[113], and future research incorporating

686 hippocampal recordings from stereoencephalography (sEEG) depth electrodes would

687 enable a more comprehensive examination of MTL structures. Such investigation,

688 combining MTL surface electrodes with hippocampus depth electrodes, could provide

689 valuable insights into how the hippocampus modulates content representations in the

690 neocortex[8].

691 **Conclusions**

692   The developing MTL is differentially involved in representations of perceptual and

693 conceptual information of visual scenes along its posterior-to-anterior axis, as

694 evidenced by distinct activity latencies and neurophysiological features. With the

695 unparalleled spatiotemporal resolution afforded by ECoG, we show that the timing of

696 HFA tracks scene onset in the posterior MTL and subjects' scene category responses in

697   the anterior MTL. Our findings further show that, in the posterior MTL, HFA predicts

698   successful memory formation and is positively linked to memory performance. In

699   contrast, in the anterior MTL, theta frequency is linked to memory performance, and

700   theta-HFA phase-amplitude coupling before subjects' scene category responses

701   predicts successful memory formation. Collectively, our findings reveal distinct

702   neurophysiological mechanisms along the MTL long axis that support the multifaceted

703   representations of episodic memory formation in children and adolescents.

MATERIALS AND METHODS

Method details

Pediatric patients

In total, 23 neurosurgical patients (12 females and 11 males; 5.9-20.5 years of age; M ± SD, 13.4 ± 4.0 years; Table S1) from the Children's Hospital of Michigan with subdural electrodes implanted for the clinical evaluation of refractory epilepsy participated in this study. Written informed consent was obtained from patients aged 18 years and older and from the guardians of subjects under 18 years. Written assent was obtained from subjects aged 13-17 years, and oral assent was obtained from younger children. This study was approved by the Institutional Review Board at Wayne State University in accordance with the Declaration of Helsinki. Among these patients, 17 patients (8 females and 9 males; 6.2-20.5 years of age; M ± SD, 13.3 ± 3.7 years) with electrode coverage in the posterior MTL, 20 patients (10 females and 10 males; 5.9-19.3 years of age; M ± SD, 13.0 ± 3.9 years) with electrode coverage in the anterior MTL, and 14 patients (6 females and 8 males; 6.2-17.1 years of age; M ± SD, 12.6 ± 3.4 years) with electrode coverage in both the posterior and anterior MTL.

Behavioral task

Subjects completed a scene recognition memory task (Fig. 1a) that has been used to study the neurophysiological mechanisms of memory with pediatric samples[36,37,40,114,115]. Pictures of scenes were presented in consecutive study-test cycles. In each study cycle, subjects studied 40 scenes of equal number of indoor and outdoor scenes, each presented 3 s following a 0.5-s fixation screen. Subjects verbalized whether each scene was "indoor" or "outdoor". Responses were coded as

36

727 correct or incorrect via offline review of individual audio recordings. Analysis of

728 electrophysiological data was restricted to studied trials with correct indoor/outdoor

729 responses. In each test cycle, subjects were tested on all 40 studied scenes, intermixed

730 with 20 new scenes as foils. Subjects were instructed to respond "old" if they

731 remembered seeing the scene and "new" if they thought they had not seen the scene in

732 the study cycle. Each scene remained on the screen until a new/old response was

733 given, following a 0.5-s fixation screen. Responses were coded as hit ("old" response to

734 studied scene), miss ("new" response to studied scene), correct rejection ("new"

735 response to foil), or false alarm ("old" response to foil). Memory performance was

736 measured with recognition accuracy, which was calculated by hit rate (number of hits

737 out of the total number of studied scenes) minus false alarm rate (number of false

738 alarms out of total number of foils). Electrophysiological data for studied scenes were

739 analyzed as a function of subsequent memory at test (i.e., subsequent hit or

740 miss)[36,37,40]. Across all 23 subjects, 43% (n = 10) completed one study-test cycle, and

741 57% (n = 13) completed two study-test cycles.

Electrode placement and localization

743   Platinum macro-electrodes (4 mm diameter, 10 mm intercontact distance) were

744 surgically implanted for extra-operative ECoG monitoring based solely on the clinical

745 needs of each patient. Three-dimensional electrode reconstructions were created by co-

746 registering post-implantation planar x-ray images of the cortical surface with

747 preoperative T1-weighted spoiled gradient-echo magnetic resonance images[64].

748 Automatic parcellation of cortical gyri was performed using FreeSurfer software[116] and

749 anatomical labels were assigned to each electrode site[117]. Subjects were included in

750   this study by artifact-free electrode coverage of the MTL, as determined by review of

751   individual reconstructions and automatic parcellation results. Electrodes were plotted on

752   MNI space for visual representation across all subjects (Fig. 2c) using the Fieldtrip

753   toolbox[118] for MATLAB (MathWorks Inc., Natick, MA).

754   *ECoG data acquisition and preprocessing*

755   ECoG data were acquired using a 192-channel Nihon Koden Neurofax 1100A

756   Digital System, sampled at 1kHz. Raw electrophysiological data were filtered with 0.1-

757   Hz high-pass and 300-Hz low-pass finite impulse response filters, and 60-Hz line noise

758   harmonics were removed using discrete Fourier transform. Continuous study data were

759   demeaned, epoched into 4.5-s trials (-1 to 3.5 s from scene onset), and manually

760   inspected blind to electrode locations and experimental task parameters. Electrodes

761   overlaying seizure onset zones[119] and electrodes and epochs displaying epileptiform

762   activity or artifactual signal (from poor contact, machine noise, etc.) were excluded.

763   Each artifact-free electrode was re-referenced to the common average of all artifact-free

764   electrodes. The re-referenced data were re-inspected to reject any trials with residual

765   noise. The final data set included a median(IQR) of 4(2) (range, 1 to 10) artifact-free

766   and nonpathological MTL electrodes and a mean ± SD of 48 ± 17 (22 to 76) study trials

767   per subject.

768

769   **Neurophysiological data analysis**

770   *High-frequency activity analysis*

771   Time-frequency representations of high-frequency activity (HFA, 70-150 Hz) were

772   quantified using a multitapering approach[120] with the FieldTrip toolbox[118]. Study trials

38

773 were zero-padded to the next power of 2 to minimize edge artifacts. The multitaper

774 frequency spectrum was then calculated by sliding a 0.25-s window in 0.025-s steps

775 across 30 logarithmically spaced, partially overlapping frequency bands centered from

776 70 to 150 Hz, with ½ fractional bandwidth at each center frequency.

777 The frequency spectrum of encoding interval (-0.15 to 3 s from scene onset) was

778 corrected on the pre-stimulus baseline interval (-0.45 to -0.15 s from scene onset) with

779 statistical bootstrapping. For each electrode and frequency, data from baseline interval

780 were pooled across all trials from which r data points (r = number of trials in that

781 subject's data) were randomly selected and averaged. This process was repeated 1000

782 times to create normal distributions of the baseline data. Power from encoding interval

783 was z-scored per time point on the pre-stimulus baseline distributions. This procedure

784 adjusts the time-frequency representations to correct for 1/f power scaling and reveals

785 event-related spectral activity[36,37,40,68,121]. The mean of the z-scored power across

786 frequencies was then taken as a single HFA time series for future analysis. The output

787 of HFA analysis was initially time-locked to scene onset. The response-locked HFA was

788 obtained by aligning the z-scored power with each trial's RT, setting the RT as time

789 zero. Subsequent memory analysis on HFA was conducted on both the stimulus-locked

790 (-0.15 to 1 s) and response-locked (-1 to 0.2 s) data.

791 HFA peak latency was analyzed on the single-trial level. Each HFA time series was

792 smoothed using a moving average with a window size of 0.05 s. HFA peak latency was

793 defined as the time point of the maximum HFA between scene onset and 0.2 s after

794 scene category response onset. The peak latency of each electrode was calculated by

795 averaging latencies across subsequent hit or miss trials for statistical modeling.

39

Oscillation detection

796

797   SpecParam was used to isolate the oscillatory component from the aperiodic 1/f

798   component[80] between 1-30 Hz. For each electrode, the power spectrum of study data

799   was calculated with Fieldtrip toolbox[118] and submitted to SpecParam for oscillation

800   detection. The power spectrum was calculated with fast Fourier transform for each study

801   trial from -0.45 to 3 s from scene onset with 2-s segment and 1.5-s overlap. Each

802   segment was zero-padded to the next power of 2 and tapered with a Hanning window to

803   minimize edge effects. The mean of the segments power spectra was then taken as

804   each trial's power spectrum. The power spectra of hit and miss trials were then

805   averaged separately for oscillation detection.

806   SpecParam models the power spectrum by initially fitting a log-logistic function to

807   capture the aperiodic component. Once parameterized, the aperiodic component is

808   subtracted from the power spectrum. The remaining data is then fitted with Gaussian

809   functions iteratively to identify and parameterize oscillatory peaks (Fig. 5a) until either

810   no peaks meet the predefined threshold or the desired number of peaks is reached.

811   Each peak is parameterized with center frequency, power, and bandwidth. The

812   SpecParam algorithm used with settings of {peak_width_limits = [2,6], max_n_peaks =

813   6, min_peak_height = 0.1, peak_threshold = 1.5, aperiodic_mode = 'fixed'}. The peak

814   with the largest power between 1-30 Hz was chosen to examine the center frequency

815   distribution. After confirming the largest oscillations clustered within the theta range (Fig.

816   5c), the largest peak between 1-10 Hz was chosen as theta oscillation for each

817   electrode. The parameterization procedure was done separately for subsequent hit and

818   miss trials.

40

819 ***Phase-amplitude coupling***

820   Intra-regional and inter-regional event-related phase-amplitude coupling (ERPAC)

821 was analyzed to capture the transient and temporal dynamics of phase-amplitude

822 coupling[122]. Study trials were padded with reflection padding and then bandpass filtered

823 at the detected theta center frequency and bandwidth and high-frequency band (70-150

824 Hz) for each electrode, separately for subsequent hit and miss trials, following the

825 removal of ERP[36,121,123]. The Hilbert transform was then used to extract phase values

826 from the theta time series and amplitude values from the high-frequency time series. To

827 evaluate the dependence of high-frequency amplitude on theta phases, the high-

828 frequency amplitude was bandpass filtered a second time at the detected theta

829 frequency and bandwidth. Phase values were extracted from this filtered signal using

830 the Hilbert transform. Phase-locking value (PLV) was then calculated as a measure of

831 ERPAC to quantify the dependence of high-frequency amplitude on theta phases[36]. For

832 inter-regional ERPAC analysis, the anterior MTL is the phase providing region and the

833 posterior MTL is the amplitude providing region. Inter-regional ERPAC was analyzed

834 between all possible anterior-posterior pairs for each subject.

835   PLV was calculated as the consistency of phase differences at each time point

836 between theta phases and the phases of theta-filtered high-frequency amplitude

837 separately across subsequent hit and miss trials. To account for differences in trial

838 counts between subsequent hit and miss trials, the raw PLV was normalized using

839 statistical bootstrapping. A surrogate PLV distribution was created by randomly shuffling

840 trial labels of theta phases and recalculating the PLV 1,000 times. The raw PLV was

841 then z-scored against the surrogate distribution[36]. ERPAC analysis was conducted on

842   data time-locked to scene onset (-1 to 3.5 s from scene onset) and to scene category

843   response onset (-1.25 to 0.25 s from response onset). Subsequent memory analysis

844   was conducted on the normalized PLV within the time window of interest (stimulus-

845   locked: -0.2 to 1 s from scene onset; response-locked: -1 to 0.2 s).

846   To identify the theta phase associated with increased high-frequency amplitude in

847   the anterior MTL, the preferred phase analysis was conducted during the time window

848   of significant SMEs in ERPAC, extending by ± 0.2 s (see Fig. 6d). For each trial, theta

849   phases were divided into 18 bins ranging from −π to π. High-frequency amplitude was

850   binned based on the theta phases and normalized to the percentage of the largest

851   binned amplitude.

Inter-regional phase coupling

853   Study trials were padded with reflection padding and then bandpass filtered at the

854   detected theta center frequency and bandwidth of each electrode, following the removal

855   of ERP[36,121,123]. The Hilbert transform was then used to extract phase values from the

856   theta time series. PLV was calculated between all posterior-anterior MTL electrode pairs

857   as a measure of phase coupling. Here, PLV quantifies the consistency of phase

858   differences between each electrode pair at each time point separately across

859   subsequent hit and miss trials. To account for differences in trial counts between

860   subsequent hit and miss trials, the raw PLV was normalized using statistical

861   bootstrapping. For each electrode pair, a surrogate PLV distribution was created by

862   randomly shuffling trial labels in one electrode and recalculating the PLV 1,000 times.

863   The raw PLV was then z-scored against the surrogate distribution[36]. Phase coupling

864   analysis was conducted on data time-locked to scene onset (-1 to 3.5 s from scene

865   onset) and to scene category response onset (-1.25 to 0.25 s from response onset).

866   Subsequent memory analysis was conducted on the normalized PLV within the time

867   window of interest (stimulus-locked: -0.2 to 1 s from scene onset; response-locked: -1 to

868   0.2 s).

869   **Statistical analysis**

870   *HFA peak latency*

871   To model HFA peak latency differences along the long axis of MTL, a linear mixed-

872   effects (LME) model with subsequent memory (i.e., hit vs. miss) and electrodes' y-

873   coordinates as fixed effects and subjects and nested electrodes as random effects was

874   used. A significant subsequent memory $\times$ y-coordinates interaction effect was followed

875   up with separate linear mixed-effects models for hit and miss, with y-coordinates as

876   fixed effects and subjects and nested electrodes as random effects.

877   To model the correlation of HFA peak latency with subjects' indoor/outdoor RT and

878   to examine if the correlation differs by region of interest (ROI; posterior vs. anterior MTL)

879   and subsequent memory (hit vs. miss), a linear mixed-effects model with ROI,

880   subsequent memory, and RT as fixed effects and subjects and nested electrodes as

881   random effects was used. A significant subsequent ROI $\times$ subsequent memory $\times$ RT

882   interaction effect was followed up with separate linear mixed-effects models for posterior

883   and anterior MTL, with subsequent memory and RT as fixed effects and subjects and

884   nested electrodes as random effects. To follow up on the significant subsequent

885   memory $\times$ RT interaction in the posterior MTL, additional models for subsequent hit and

886   miss were conducted with RT as fixed effect and subjects and nested electrodes as

887   random effects.

43

888 ***Theta parameters***

889   After detecting and parameterizing theta oscillations between 1-10 Hz for each

890   electrode, LME models were used to test if theta parameters (i.e., theta frequency,

891   power, and bandwidth) differ by regions and subsequent memory. For each theta

892   parameter, a LME model was conducted with regions and subsequent memory as fixed

893   effects and subjects and nested electrodes as random effects.

894   To examine the individual differences in theta parameters for each region, LME

895   models were conducted separately for the posterior and anterior MTL. For each theta

896   parameter, LME was run with subsequent memory, recognition accuracy, and age as

897   fixed effects and subjects and nested electrodes as random effects.

898   ***Subsequent memory effects (SMEs)***

899   SMEs were analyzed on HFA, phase-amplitude coupling, and phase coupling data

900   to test the differences between subsequent hit and miss trials. For each region and

901   measure, subsequent memory analysis was conducted with an LME model and cluster-

902   based correction was used to correct for multiple comparisons. LME was conducted for

903   each time point with subsequent memory as fixed effects and subjects and nested

904   electrodes as random effects. To correct for multiple comparisons, the hit and miss trial

905   labels were randomly shuffled within each electrode and the model was re-run. This

906   procedure was repeated 1,000 times. The size of the maximum cluster of significant

907   SMEs ($p < 0.05$) from each run was extracted to create the random permutation

908   distribution. The cluster size of the observed SMEs ($p < 0.05$) was compared against

909   the random permutation distribution to obtain the corrected p-value of each subsequent

910   memory cluster[36,124]. SMEs that survived the cluster-based correction (corrected p <

44

911   0.05) were reported. To disentangle the scene-induced and response-related effects,

912   the subsequent memory analysis was conducted on the data locked to scene onset and

913   locked to scene category response onset.

914   ***Inter-individual differences in subsequent memory effects***

915   Multiple regression analyses were conducted with recognition accuracy and age as

916   predictors to investigate behavioral relevance and age-related differences of the

917   SMEs[36,40]. The differences between subsequent hit and miss were averaged across

918   electrodes for each subject and across the time window of each significant subsequent

919   memory cluster (corrected $p < 0.05$) and submitted to multiple regression with

920   recognition accuracy and age as predictors.

921   ***Correlation between posterior MTL HFA and anterior MTL theta parameters***

922   The Pearson correlation between posterior MTL HFA and anterior MTL theta

923   parameters (i.e., frequency, power, and bandwidth) was calculated to assess the

924   association between the distinct neurophysiological features in the posterior and

925   anterior MTL. Posterior HFA was obtained separately for subsequent hit and miss trials

926   by averaging HFA within the time window of significant SMEs (Fig. 4a). The Pearson

927   correlation was then calculated between the posterior HFA and the anterior MTL theta

928   parameters separately for subsequent hit and miss trials.

Data Availability

De-identified raw data are deposited to the NIMH public database (DOI pending

acceptance). Additional data related to the paper may be requested from the authors.

Code Availability

Custom code used for the analyses in this study is available at GitHub:

https://github.com/qinyin07/mtl_long_axis.

Acknowledgements

Author Contributions

Conceptualization: Q.Y., N.O., and E.L.J.; Methodology: N.O., Q.Y., and E.L.J.;

Software: Q.Y., E.L.J., and A.J.D.; Validation: Q.Y., N.O., and E.L.J.; Formal analysis:

Q.Y.; Investigation: N.O., E.A., E.L.J., and R.T.K.; Resources: N.O. and E.L.J.; Data

curation: Q.Y., E.L.J., and N.O.; Visualization: Q.Y. and E.L.J; Writing - original draft:

Q.Y.; Writing - review and editing: Q.Y., N.O., E.L.J., R.T.K., and A.J.D.; Supervision:

N.O.; Project administration: N.O., E.L.J., and Q.Y.; Funding acquisition: N.O., E.L.J.,

R.T.K., and E.A.

Competing Interests

None.

References:

951 1. Cycowicz, Y. M., Friedman, D., Snodgrass, J. G. & Duff, M. Recognition and source memory for pictures in children and adults. *Neuropsychologia* **39**, 255–267 (2001).

954 2. Dirks, J. & Neisser, U. Memory for objects in real scenes: The development of recognition and recall. *Journal of Experimental Child Psychology* **23**, 315–328 (1977).

957 3. Ofen, N. The development of neural correlates for memory formation. *Neuroscience and Biobehavioral Reviews* **36**, 1708–1717 (2012).

959 4. Ofen, N. & Shing, Y. L. From perception to memory: Changes in memory systems across the lifespan. *Neuroscience and Biobehavioral Reviews* **37**, 2258–2267 (2013).

962 5. Scoville, W. B. & Milner, B. Loss of Recent Memory After Bilateral Hippocampal Lesions. *Journal of Neurology, Neurosurgery & Psychiatry* **20**, 11–21 (1957).

964 6. Squire, L. R. Memory and the Hippocampus: A Synthesis From Findings With Rats, Monkeys, and Humans. *Psychological Review* **99**, 195–213 (1992).

966 7. Diana, R. A., Yonelinas, A. P. & Ranganath, C. Imaging recollection and familiarity in the medial temporal lobe: a three-component model. *Trends in Cognitive Sciences* **11**, 379–386 (2007).

969 8. Ranganath, C. & Ritchey, M. Two cortical systems for memory-guided behaviour. *Nature Reviews Neuroscience* **13**, 713–726 (2012).

971 9. Robin, J., Rai, Y., Valli, M. & Olsen, R. K. Category specificity in the medial temporal lobe: A systematic review. *Hippocampus* **29**, 313–339 (2019).

973   10. Kahn, I., Andrews-Hanna, J. R., Vincent, J. L., Snyder, A. Z. & Buckner, R. L. Distinct

974   Cortical Anatomy Linked to Subregions of the Medial Temporal Lobe Revealed by

975   Intrinsic Functional Connectivity. *Journal of Neurophysiology* **100**, 129–139 (2008).

976   11. Qin, S. *et al.* Large-scale intrinsic functional network organization along the long axis

977   of the human medial temporal lobe. *Brain Struct Funct* **221**, 3237–3258 (2016).

978   12. Reznik, D., Trampel, R., Weiskopf, N., Witter, M. P. & Doeller, C. F. Dissociating

979   distinct cortical networks associated with subregions of the human medial temporal

980   lobe using precision neuroimaging. *Neuron* **111**, 2756-2772.e7 (2023).

981   13. Suzuki, W. A. Perception and the Medial Temporal Lobe: Evaluating the Current

982   Evidence. *Neuron* **61**, 657–666 (2009).

983   14. Suzuki, W. A. & Amaral, D. G. Perirhinal and parahippocampal cortices of the

984   macaque monkey: Cortical afferents. *Journal of Comparative Neurology* **350**, 497–

985   533 (1994).

986   15. Suzuki, W. A. & Naya, Y. The Perirhinal Cortex. *Annual Review of Neuroscience* **37**,

987   39–53 (2014).

988   16. Barense, M. D. *et al.* Functional Specialization in the Human Medial Temporal Lobe.

989   *J. Neurosci.* **25**, 10239–10246 (2005).

990   17. Barense, M. D., Gaffan, D. & Graham, K. S. The human medial temporal lobe

991   processes online representations of complex objects. *Neuropsychologia* **45**, 2963–

992   2974 (2007).

993   18. Bohbot, V. D. *et al.* Spatial memory deficits in patients with lesions to the right

994   hippocampus and to the right parahippocampal cortex. *Neuropsychologia* **36**,

995   1217–1238 (1998).

996   19. Epstein, R., DeYoe, E. A., Press, D. Z., Rosen, A. C. & Kanwisher, N.

997   Neuropsychological evidence for a topographical learning mechanism in

998   parahippocampal cortex. *Cognitive Neuropsychology* **18**, 481–508 (2001).

999   20. Lee, A. C. H. *et al.* Specialization in the medial temporal lobe for processing of

1000   objects and scenes. *Hippocampus* **15**, 782–797 (2005).

1001   21. Lee, A. C. H. *et al.* Perceptual deficits in amnesia: challenging the medial temporal

1002   lobe 'mnemonic' view. *Neuropsychologia* **43**, 1–11 (2005).

1003   22. Liang, J. C., Wagner, A. D. & Preston, A. R. Content Representation in the Human

1004   Medial Temporal Lobe. *Cerebral Cortex* **23**, 80–96 (2013).

1005   23. Litman, L., Awipi, T. & Davachi, L. Category-specificity in the human medial temporal

1006   lobe cortex. *Hippocampus* **19**, 308–319 (2009).

1007   24. Buffalo, E. A., Bellgowan, P. S. F. & Martin, A. Distinct roles for medial temporal lobe

1008   structures in memory for objects and their locations. *Learn. Mem.* **13**, 638–643

1009   (2006).

1010   25. Diana, R. A., Yonelinas, A. P. & Ranganath, C. High-resolution multi-voxel pattern

1011   analysis of category selectivity in the medial temporal lobes. *Hippocampus* **18**,

1012   536–541 (2008).

1013   26. Preston, A. R. *et al.* High-resolution fMRI of content-sensitive subsequent memory

1014   responses in human medial temporal lobe. *Journal of Cognitive Neuroscience* **22**,

1015   156–173 (2010).

1016   27. Fiorilli, J. *et al.* Reconciling the object and spatial processing views of the perirhinal

1017   cortex through task-relevant unitization. *Hippocampus* **31**, 737–755 (2021).

1018   28. Kivisaari, S. L., Probst, A. & Taylor, K. I. The Perirhinal, Entorhinal, and

1019   Parahippocampal Cortices and Hippocampus: An Overview of Functional Anatomy

1020   and Protocol for Their Segmentation in MR Images. in *fMRI: Basics and Clinical*

1021   *Applications* (eds Ulmer, S. & Jansen, O.) 355–383 (Springer International

1022   Publishing, Cham, 2020). doi:10.1007/978-3-030-41874-8_24.

1023   29. Ritchey, M., Libby, L. A. & Ranganath, C. Chapter 3 - Cortico-hippocampal systems

1024   involved in memory and cognition: the PMAT framework. in *Progress in Brain*

1025   *Research* (eds O'Mara, S. & Tsanov, M.) vol. 219 45–64 (Elsevier, 2015).

1026   30. Mormann, F. *et al.* Latency and Selectivity of Single Neurons Indicate Hierarchical

1027   Processing in the Human Medial Temporal Lobe. *J. Neurosci.* **28**, 8865–8872

1028   (2008).

1029   31. Ofen, N. *et al.* Development of the declarative memory system in the human brain.

1030   *Nature Neuroscience* **10**, 1198–1205 (2007).

1031   32. Shing, Y. L., Brehmer, Y., Heekeren, H. R., Bäckman, L. & Lindenberger, U. Neural

1032   activation patterns of successful episodic encoding: Reorganization during

1033   childhood, maintenance in old age. *Developmental Cognitive Neuroscience* **20**, 59–

1034   69 (2016).

1035   33. Chai, X. J., Ofen, N., Jacobs, L. F. & Gabrieli, J. D. E. Scene complexity: Influence

1036   on perception, memory, and development in the medial temporal lobe. *Frontiers in*

1037   *Human Neuroscience* **4**, (2010).

1038   34. Golarai, G. *et al.* Differential development of high-level visual cortex correlates with

1039   category-specific recognition memory. *Nature Neuroscience* **10**, 512–522 (2007).

1040   35. Ghetti, S., DeMaster, D. M., Yonelinas, A. P. & Bunge, S. A. Developmental

1041   differences in medial temporal lobe function during memory encoding. *Journal of*

1042   *Neuroscience* **30**, 9548–9556 (2010).

1043   36. Johnson, E. L. *et al.* Dissociable oscillatory theta signatures of memory formation in

1044   the developing brain. *Current Biology* 1–13 (2022) doi:10.1016/j.cub.2022.01.053.

1045   37. Johnson, E. L., Tang, L., Yin, Q., Asano, E. & Ofen, N. Direct brain recordings reveal

1046   prefrontal cortex dynamics of memory development. *Science Advances* **4**, (2018).

1047   38. Tang, L. *et al.* Differential Functional Connectivity in Anterior and Posterior

1048   Hippocampus Supporting the Development of Memory Formation. *Frontiers in*

1049   *Human Neuroscience* **14**, 1–16 (2020).

1050   39. Tang, L., Shafer, A. T. & Ofen, N. Prefrontal Cortex Contributions to the Development

1051   of Memory Formation. *Cerebral Cortex* **28**, 3295–3308 (2018).

1052   40. Yin, Q. *et al.* Direct brain recordings reveal occipital cortex involvement in memory

1053   development. *Neuropsychologia* **148**, 107625 (2020).

1054   41. Ofen, N., Tang, L., Yu, Q. & Johnson, E. L. Memory and the developing brain: From

1055   description to explanation with innovation in methods. *Developmental Cognitive*

1056   *Neuroscience* **36**, 100613 (2019).

1057   42. Yin, Q., Johnson, E. L. & Ofen, N. Neurophysiological mechanisms of cognition in

1058   the developing brain: Insights from intracranial EEG studies. *Developmental*

1059   *Cognitive Neuroscience* **64**, 101312 (2023).

1060   43. Fedele, T. *et al.* The relation between neuronal firing, local field potentials and

1061   hemodynamic activity in the human amygdala in response to aversive dynamic

1062   visual stimuli. *NeuroImage* **213**, 116705 (2020).

1063   44. Leszczyński, M. *et al.* Dissociation of broadband high-frequency activity and

1064   neuronal firing in the neocortex. *Science Advances* **6**, eabb0977 (2020).

1065   45. Nir, Y. *et al.* Coupling between Neuronal Firing Rate, Gamma LFP, and BOLD fMRI

1066   Is Related to Interneuronal Correlations. *Current Biology* **17**, 1275–1285 (2007).

1067   46. Watson, B. O., Ding, M. & Buzsáki, G. Temporal coupling of field potentials and

1068   action potentials in the neocortex. *European Journal of Neuroscience* **48**, 2482–

1069   2497 (2018).

1070   47. Leonard, M. K. *et al.* Large-scale single-neuron speech sound encoding across the

1071   depth of human cortex. *Nature* **626**, 593–602 (2024).

1072   48. Haufe, S. *et al.* Elucidating relations between fMRI, ECoG, and EEG through a

1073   common natural stimulus. *NeuroImage* **179**, 79–91 (2018).

1074   49. Hermes, D. *et al.* Neurophysiologic correlates of fMRI in human motor cortex.

1075   *Human Brain Mapping* **33**, 1689–1699 (2012).

1076   50. Jacques, C. *et al.* Corresponding ECoG and fMRI category-selective signals in

1077   human ventral temporal cortex. *Neuropsychologia* **83**, 14–28 (2016).

1078   51. Herweg, N. A., Solomon, E. A. & Kahana, M. J. Theta Oscillations in Human

1079   Memory. *Trends in Cognitive Sciences* **24(3)**, 208–227 (2020).

1080   52. Herweg, N. A. & Kahana, M. J. Spatial representations in the human brain. *Frontiers*

1081   *in Human Neuroscience* **12**, 1–16 (2018).

1082   53. Johnson, E. L., Kam, J., Tzovara, A. & Knight, R. T. Insights into human cognition

1083   from intracranial EEG: A review of audition, memory, internal cognition, and

1084   causality. *Journal of Neural Engineering* (2020) doi:10.1088/1741-2552/abb7a5.

1085   54. Seger, S. E., Kriegel, J. L. S., Lega, B. C. & Ekstrom, A. D. Memory-related

1086   processing is the primary driver of human hippocampal theta oscillations. *Neuron*

1087   S0896627323004749 (2023) doi:10.1016/j.neuron.2023.06.015.

1088   55. Buzsáki, G. Theta rhythm of navigation: Link between path integration and landmark

1089   navigation, episodic and semantic memory. *Hippocampus* **15**, 827–840 (2005).

1090   56. Buzsáki, G. & Moser, E. I. Memory, navigation and theta rhythm in the hippocampal-

1091   entorhinal system. *Nature Neuroscience* **16**, 130–138 (2013).

1092   57. Lisman, J. & Jensen, O. The Theta-Gamma Neural Code. *Neuron* **77**, 1002–1016

1093   (2013).

1094   58. Buzsaki, G. & Draguhn, A. Neuronal Oscillations in Cortical Networks. *Science* **304**,

1095   1926–1929 (2004).

1096   59. Fries, P. Rhythms for Cognition: Communication through Coherence. *Neuron* **88**,

1097   220–235 (2015).

1098   60. Helfrich, R. F. & Knight, R. T. Oscillatory Dynamics of Prefrontal Cognitive Control.

1099   *Trends in Cognitive Sciences* **20**, 916–930 (2016).

1100   61. Nyhus, E. & Curran, T. Functional role of gamma and theta oscillations in episodic

1101   memory. *Neuroscience and Biobehavioral Reviews* **34**, 1023–1035 (2010).

1102   62. Fries, P. A mechanism for cognitive dynamics: Neuronal communication through

1103   neuronal coherence. *Trends in Cognitive Sciences* **9**, 474–480 (2005).

1104   63. Johnson, E. L. & Knight, R. T. How Can iEEG Be Used to Study Inter-Individual and

1105   Developmental Differences? in *Intracranial EEG: A Guide for Cognitive*

1106   *Neuroscientists* (ed. Axmacher, N.) 143–154 (Springer International Publishing,

1107   Cham, 2023). doi:10.1007/978-3-031-20910-9_10.

1108   64. Nakai, Y. *et al.* Three- and four-dimensional mapping of speech and language in

1109   patients with epilepsy. *Brain* **140**, 1351–1370 (2017).

1110   65. Burke, J. F. *et al.* Human intracranial high-frequency activity maps episodic memory

1111   formation in space and time. *NeuroImage* **85**, 834–843 (2014).

1112   66. Greenberg, J. A., Burke, J. F., Kahana, M. J. & Zaghloul, K. A. Decreases in theta

1113   and increases in high frequency activity underlie associative memory encoding.

1114   *NeuroImage* **114**, 257–263 (2015).

1115   67. Kucewicz, M. T. *et al.* Human Verbal Memory Encoding Is Hierarchically Distributed

1116   in a Continuous Processing Stream. *eNeuro* **6**, e0214-18.2018 (2019).

1117   68. Flinker, A. *et al.* Redefining the role of Broca's area in speech. *Proceedings of the*

1118   *National Academy of Sciences* **112**, 2871–2875 (2015).

1119   69. Frauscher, B. *et al.* Atlas of the normal intracranial electroencephalogram:

1120   neurophysiological awake activity in different cortical areas. *Brain* 1–15 (2018)

1121   doi:10.1093/brain/awy035.

1122   70. Mahjoory, K., Schoffelen, J.-M., Keitel, A. & Gross, J. The frequency gradient of

1123   human resting-state brain oscillations follows cortical hierarchies. *eLife* **9**, e53715

1124   (2020).

1125   71. Zhang, H., Watrous, A. J., Patel, A. & Jacobs, J. Theta and Alpha Oscillations Are

1126   Traveling Waves in the Human Neocortex. *Neuron* **98**, 1269-1281.e4 (2018).

1127   72. Haegens, S., Cousijn, H., Wallis, G., Harrison, P. J. & Nobre, A. C. Inter- and intra-

1128   individual variability in alpha peak frequency. *NeuroImage* **92**, 46–55 (2014).

1129 73. Mierau, A., Klimesch, W. & Lefebvre, J. State-dependent alpha peak frequency
1130   shifts: Experimental evidence, potential mechanisms and functional implications.
1131   *Neuroscience* **360**, 146–154 (2017).

1132 74. Freschl, J., Azizi, L. A., Balboa, L., Kaldy, Z. & Blaser, E. The development of peak
1133   alpha frequency from infancy to adolescence and its role in visual temporal
1134   processing: A meta-analysis. *Developmental Cognitive Neuroscience* **57**, 101146
1135   (2022).

1136 75. Miskovic, V. *et al.* Developmental changes in spontaneous electrocortical activity
1137   and network organization from early to late childhood. *NeuroImage* **118**, 237–247
1138   (2015).

1139 76. Schaworonkow, N. & Voytek, B. Longitudinal changes in aperiodic and periodic
1140   activity in electrophysiological recordings in the first seven months of life.
1141   *Developmental Cognitive Neuroscience* **47**, 100895 (2021).

1142 77. Dustman, R. E., Shearer, D. E. & Emmerson, R. Y. EEG and event-related potentials
1143   in normal aging. *Progress in Neurobiology* **41**, 369–401 (1993).

1144 78. Merkin, A. *et al.* Do age-related differences in aperiodic neural activity explain
1145   differences in resting EEG alpha? *Neurobiology of Aging* **121**, 78–87 (2023).

1146 79. Scally, B., Burke, M. R., Bunce, D. & Delvenne, J.-F. Resting-state EEG power and
1147   connectivity are associated with alpha peak frequency slowing in healthy aging.
1148   *Neurobiology of Aging* **71**, 149–155 (2018).

1149 80. Donoghue, T. *et al.* Parameterizing neural power spectra into periodic and aperiodic
1150   components. *Nature Neuroscience* **23**, 1655–1665 (2020).

1151   81. Johnson, E. L. *et al.* A rapid theta network mechanism for flexible information

1152   encoding. *Nat Commun* **14**, 2872 (2023).

1153   82. Hasselmo, M. E. & Stern, C. E. Theta rhythm and the encoding and retrieval of

1154   space and time. *NeuroImage* **85**, 656–666 (2014).

1155   83. Saint Amour di Chanaz, L. *et al.* Gamma amplitude is coupled to opposed

1156   hippocampal theta-phase states during the encoding and retrieval of episodic

1157   memories in humans. *Current Biology* **33**, 1836-1843.e6 (2023).

1158   84. Yoo, H. B., Umbach, G. & Lega, B. Neurons in the human medial temporal lobe

1159   track multiple temporal contexts during episodic memory processing. *NeuroImage*

1160   **245**, 118689 (2021).

1161   85. Brainerd, C. J. & Reyna, V. F. Fuzzy-trace theory and memory development.

1162   *Developmental Review* **24**, 396–439 (2004).

1163   86. Grilli, M. D. & Sheldon, S. Autobiographical event memory and aging: older adults

1164   get the gist. *Trends in Cognitive Sciences* **26**, 1079–1089 (2022).

1165   87. Robin, J. & Moscovitch, M. Details, gist and schema: hippocampal–neocortical

1166   interactions underlying recent and remote episodic and spatial memory. *Current*

1167   *Opinion in Behavioral Sciences* **17**, 114–123 (2017).

1168   88. Grill-Spector, K. & Malach, R. The human visual cortex. *Annual Review of*

1169   *Neuroscience* 649–677 (2004) doi:10.1146/annurev.neuro.27.070203.144220.

1170   89. Hasson, U., Chen, J. & Honey, C. J. Hierarchical process memory: memory as an

1171   integral component of information processing. *Trends in Cognitive Sciences* **19**,

1172   304–313 (2015).

1173   90. Quiroga, R. Q. Concept cells: the building blocks of declarative memory functions.

1174   *Nat Rev Neurosci* **13**, 587–597 (2012).

1175   91. Quiroga, R. Q., Reddy, L., Kreiman, G., Koch, C. & Fried, I. Invariant visual

1176   representation by single neurons in the human brain. *Nature* **435**, 1102–1107

1177   (2005).

1178   92. Suthana, N. & Fried, I. Percepts to recollections: insights from single neuron

1179   recordings in the human brain. *Trends in Cognitive Sciences* **16**, 427–436 (2012).

1180   93. Hanslmayr, S., Staresina, B. P. & Bowman, H. Oscillations and Episodic Memory:

1181   Addressing the Synchronization/Desynchronization Conundrum. *Trends in*

1182   *Neurosciences* **39**, 16–25 (2016).

1183   94. Goyal, A. *et al.* Functionally distinct high and low theta oscillations in the human

1184   hippocampus. *Nature Communications* 498055 (2020) doi:10.1101/498055.

1185   95. Richard, G. R. *et al.* Speed modulation of hippocampal theta frequency correlates

1186   with spatial memory performance. *Hippocampus* **23**, 1269–1279 (2013).

1187   96. Moran, R. J. *et al.* Peak Frequency in the Theta and Alpha Bands Correlates with

1188   Human Working Memory Capacity. *Front. Hum. Neurosci.* **4**, (2010).

1189   97. O'Keefe, J. & Recce, M. L. Phase relationship between hippocampal place units and

1190   the EEG theta rhythm. *Hippocampus* **3**, 317–330 (1993).

1191   98. Lega, B. C., Burke, J., Jacobs, J. & Kahana, M. J. Slow-Theta-to-Gamma Phase-

1192   Amplitude Coupling in Human Hippocampus Supports the Formation of New

1193   Episodic Memories. *Cerebral Cortex* **26**, 268–278 (2016).

1194   99. Rutishauser, U., Ross, I. B., Mamelak, A. N. & Schuman, E. M. Human memory

1195   strength is predicted by theta-frequency phase-locking of single neurons. *Nature*

1196   **464**, 903–907 (2010).

1197   100. Canolty, R. T. *et al.* High gamma power is phase-locked to theta oscillations in

1198   human neocortex. *Science* **313**, 1626–1628 (2006).

1199   101. Solomon, E. A. *et al.* Widespread theta synchrony and high-frequency

1200   desynchronization underlies enhanced cognition. *Nature Communications* **8**,

1201   (2017).

1202   102. Solomon, E. A. *et al.* Dynamic Theta Networks in the Human Medial Temporal Lobe

1203   Support Episodic Memory. *Current Biology* **29**, 1100-1111.e4 (2019).

1204   103. Axmacher, N., Mormann, F., Fernández, G., Elger, C. E. & Fell, J. Memory

1205   formation by neuronal synchronization. *Brain Research Reviews* **52**, 170–182

1206   (2006).

1207   104. Wang, D. X., Schmitt, K., Seger, S., Davila, C. E. & Lega, B. C. Cross-regional

1208   phase amplitude coupling supports the encoding of episodic memories.

1209   *Hippocampus* 1–12 (2021) doi:10.1002/hipo.23309.

1210   105. Sander, M. C., Werkle-Bergner, M., Gerjets, P., Shing, Y. L. & Lindenberger, U. The

1211   two-component model of memory development, and its potential implications for

1212   educational settings. *Developmental Cognitive Neuroscience* **2**, S67–S77 (2012).

1213   106. Fandakova, Y., Leckey, S., Driver, C. C., Bunge, S. A. & Ghetti, S. Neural specificity

1214   of scene representations is related to memory performance in childhood.

1215   *NeuroImage* **199**, 105–113 (2019).

1216 107. Libby, L. A., Ekstrom, A. D., Ragland, J. D. & Ranganath, C. Differential

1217   Connectivity of Perirhinal and Parahippocampal Cortices within Human

1218   Hippocampal Subregions Revealed by High-Resolution Functional Imaging. *J.*

1219   *Neurosci.* **32**, 6550–6560 (2012).

1220 108. Wisse, L. E. M. *et al.* A harmonized segmentation protocol for hippocampal and

1221   parahippocampal subregions: Why do we need one and what are the key goals?

1222   *Hippocampus* **27**, 3–11 (2017).

1223 109. Wuestefeld, A. *et al.* Comparison of histological delineations of medial temporal

1224   lobe cortices by four independent neuroanatomy laboratories. *Hippocampus* **34**,

1225   241–260 (2024).

1226 110. Insausti, R. *et al.* MR volumetric analysis of the human entorhinal, perirhinal, and

1227   temporopolar cortices. *American Journal of Neuroradiology* **19**, 659–671 (1998).

1228 111. Olsen, R. K. *et al.* Performance-Related Sustained and Anticipatory Activity in

1229   Human Medial Temporal Lobe during Delayed Match-to-Sample. *J. Neurosci.* **29**,

1230   11880–11890 (2009).

1231 112. Pruessner, J. C. *et al.* Volumetry of Temporopolar, Perirhinal, Entorhinal and

1232   Parahippocampal Cortex from High-resolution MR Images: Considering the

1233   Variability of the Collateral Sulcus. *Cerebral Cortex* **12**, 1342–1353 (2002).

1234 113. Poppenk, J., Evensmoen, H. R., Moscovitch, M. & Nadel, L. Long-axis

1235   specialization of the human hippocampus. *Trends in Cognitive Sciences* **17**, 230–

1236   240 (2013).

1237 114. Rau, E. M. B. *et al.* Reinstatement and transformation of memory traces for

1238   recognition. *Science Advances* **11**, eadp9336 (2025).

1239   115. Cross, Z. R. *et al.* The development of aperiodic neural activity in the human brain.

1240   *Nat Hum Behav* 1–16 (2025) doi:10.1038/s41562-025-02270-x.

1241   116. Desikan, R. S. *et al.* An automated labeling system for subdividing the human

1242   cerebral cortex on MRI scans into gyral based regions of interest. *NeuroImage* **31**,

1243   698–980 (2006).

1244   117. Pieters, T. A., Conner, C. R. & Tandon, N. Recursive grid partitioning on a cortical

1245   surface model: an optimized technique for the localization of implanted subdural

1246   electrodes. *Journal of Neurosurgery* **118**, 1086–1097 (2013).

1247   118. Oostenveld, R., Fries, P., Maris, E. & Schoffelen, J. M. FieldTrip: Open source

1248   software for advanced analysis of MEG, EEG, and invasive electrophysiological

1249   data. *Computational Intelligence and Neuroscience* **2011**, 156869 (2011).

1250   119. Asano, E., Juhsz, C., Shah, A., Sood, S. & Chugani, H. T. Role of subdural

1251   electrocorticography in prediction of long-term seizure outcome in epilepsy surgery.

1252   *Brain* **132**, 1038–1047 (2009).

1253   120. Mitra, P. P. & Pesaran, B. Analysis of dynamic brain imaging data. *Biophysical*

1254   *journal* **76**, 691–708 (1999).

1255   121. Johnson, E. L. *et al.* Bidirectional Frontoparietal Oscillatory Systems Support

1256   Working Memory. *Current Biology* **27**, 1829-1835.e4 (2017).

1257   122. Voytek, B., D'Esposito, M., Crone, N. & Knight, R. T. A method for event-related

1258   phase/amplitude coupling. *NeuroImage* **64**, 416–424 (2013).

1259   123. Johnson, E. L. *et al.* Dynamic frontotemporal systems process space and time in

1260   working memory. *PLoS Biology* 1–22 (2018).

1261   124. Dede, A. J. O. *et al.* Declarative Memory Through the Lens of Single-Trial Peaks in

1262   High-Frequency Power. 2025.01.02.631123 Preprint at

1263   https://doi.org/10.1101/2025.01.02.631123 (2025).

1264